

THIN SECTION HIGH COOLING RATE SOLIDIFICATION,  
THERMOMECHANICAL PROCESSING AND CHARACTERIZATION OF AISI  
DC53 COLD WORK TOOL STEEL

A THESIS SUBMITTED TO  
THE GRADUATE SCHOOL OF NATURAL AND APPLIED SCIENCES  
OF  
MIDDLE EAST TECHNICAL UNIVERSITY

BY

İSMAİL SEÇKİN ÇARDAKLI

IN PARTIAL FULFILLMENT OF THE REQUIREMENTS  
FOR  
THE DEGREE OF DOCTOR OF PHILOSOPHY  
IN  
METALLURGICAL AND MATERIALS ENGINEERING

SEPTEMBER 2019



Approval of the thesis:

**THIN SECTION HIGH COOLING RATE SOLIDIFICATION,  
THERMOMECHANICAL PROCESSING AND CHARACTERIZATION OF  
AISI DC53 COLD WORK TOOL STEEL**

submitted by **İSMAİL SEÇKİN ÇARDAKLI** in partial fulfillment of the requirements for the degree of **Doctor of Philosophy in Metallurgical and Materials Engineering Department, Middle East Technical University** by,

Prof. Dr. Halil Kalıpçılar  
Dean, Graduate School of **Natural and Applied Sciences**

\_\_\_\_\_

Prof. Dr. Cemil Hakan Gür  
Head of Department, **Met. and Mat. Eng.**

\_\_\_\_\_

Prof. Dr. Ali Kalkanlı  
Supervisor, **Met. and Mat. Eng., METU**

\_\_\_\_\_

**Examining Committee Members:**

Prof. Dr. Bilgehan Ögel  
Met. and Mat. Eng., METU

\_\_\_\_\_

Prof. Dr. Ali Kalkanlı  
Met. and Mat. Eng., METU

\_\_\_\_\_

Prof. Dr. Abbas Tamer Özdemir  
Met. and Mat. Eng., Gazi University

\_\_\_\_\_

Assoc. Prof. Dr. Ender Keskinliç  
Met. and Mat. Eng., Atılım University

\_\_\_\_\_

Assist. Prof. Dr. Erkan Konca  
Met. and Mat. Eng., Atılım University

\_\_\_\_\_

Date: 05.09.2019

**I hereby declare that all information in this document has been obtained and presented in accordance with academic rules and ethical conduct. I also declare that, as required by these rules and conduct, I have fully cited and referenced all material and results that are not original to this work.**

Name, Surname: İsmail Seçkin Çardaklı

Signature:

## ABSTRACT

### **THIN SECTION HIGH COOLING RATE SOLIDIFICATION, THERMOMECHANICAL PROCESSING AND CHARACTERIZATION OF AISI DC53 COLD WORK TOOL STEEL**

Çardaklı, İsmail Seçkin  
Doctor of Philosophy, Metallurgical and Materials Engineering  
Supervisor: Prof. Dr. Ali Kalkanlı

September 2019, 79 pages

In this study, firstly, the solidification behaviour of AISI DC53 cold work tool steel was investigated by means of a cooling curve and its first derivative. Copper and sand wedge-shaped moulds were used to obtain various solidification rates. To reveal the cooling rate degree during solidification, the secondary dendrite arm spacing of the steel alloy was examined by scanning electron microscopy (SEM). The solidification rates of each section for both wedge steel samples were calculated by means of the secondary dendrite arm spacing using a research-based empirical relation from the literature. Secondly, as alternative method to conventional production methods involving thin section copper permanent mould casting (fast solidification) and water atomization (rapid solidification) of AISI DC53 cold work tool steel have been investigated. Thin slabs obtained by copper mould casting was homogenized at 1150°C for one hour and then hot rolling was be applied. After hot rolling, conventional heat treatment has been applied to thin slabs. The same heat treatment procedure has been performed for a commercially available AISI DC53 which is manufactured by thick section ingot casting and rolling. In order to investigate also the effect of rapid solidification on AISI DC53 tool steel, steel powder was produced by water atomization technique. Experimental results revealed that at the tip region of

the cast specimen in the copper wedge shaped mould, the carbide size was 7–8  $\mu\text{m}$ , where the solidification rate was approximately  $4,830\text{ }^{\circ}\text{C}\cdot\text{s}^{-1}$ . Thin steel slabs in permanent copper mould and rapidly solidified tool steel powder by water atomization have a more refined primary  $\text{M}_7\text{C}_3$  carbides than commercially available steel.

Keywords: Cold Work Tool Steel, High Cooling Rate Solidification, Primary Carbides, Permanent Mold Casting

## ÖZ

### **AISI DC53 SOĞUK İŞ TAKIM ÇELİĞİNİN İNCE KESİT HIZLI KATILAŞMASI, TERMOMEKANİK SÜRECİ VE KARAKTERİZASYONU**

Çardaklı, İsmail Seçkin  
Doktora, Metalurji ve Malzeme Mühendisliği  
Tez Danışmanı: Prof. Dr. Ali Kalkanlı

Eylül 2019, 79 sayfa

Bu çalışmada ilk olarak AISI DC53 soğuk iş takım çeliğinin katılma davranışı bir soğuma eğrisi ve onun ilk türevi ile incelenmiştir. Çeşitli katılma hızları elde etmek için bakır ve kum kama şeklindeki kalıplar kullanılmıştır. Katılma sırasındaki soğuma hızı derecesini ortaya çıkarmak için, çelik alaşımın ikincil dendrit kol aralığı taramalı elektron mikroskobu (SEM) ile incelenmiştir. Her iki kama çelik numunesi için her bir bölümün katılma hızları, literatürden araştırmaya dayalı bir ampirik ilişki kullanılarak ikincil dendrit kol aralığı vasıtasıyla hesaplanmıştır. İkinci olarak, AISI DC53 soğuk iş takım çeliğinin ince kesitli bakır kalıp dökümünü (hızlı katılma) ve su atomizasyonunu (ani katılma) içeren geleneksel üretim yöntemlerine alternatif bir yöntem olarak incelenmiştir. Bakır kalıp dökümü ile elde edilen ince plakalar 1150°C'de bir saat homojenize edildi ve sonra sıcak haddeleme uygulandı. Sıcak haddelemeden sonra, ince plakalara geleneksel ısıtma işlemi uygulanmıştır. Aynı ısıtma işlemi prosedürü, kalın kesitli külçe döküm ve haddeleme ile üretilen, ticari olarak temin edilebilen bir AISI DC53 için gerçekleştirilmiştir. Ani katılmanın AISI DC53 takım çeliği üzerindeki etkisini de araştırmak için, su atomizasyon tekniği ile çelik tozu üretildi. Deneysel sonuçlar, bakır numunenin bakır kama şeklindeki kalıptaki döküm numunesinin uç bölgesinde karbür boyutunun 7-8 um olduğunu ve katılma hızının yaklaşık  $4.830 \text{ } ^\circ\text{C} \cdot \text{s}^{-1}$  olduğunu gösterdi. Bakır kalıpta ince çelik plakalar ve

su atomizasyonu ile hızla katılařan takım eliđi tozu, ticari olarak temin edilebilen elikten daha rafine birincil  $M_7C_3$  karbrlere sahiptir.

Anahtar Kelimeler: Sođuk İř Takım eliđi, Yksek Hızlı Katılařma, Birincil Karbrlar, Kokil Dkm



To My Beloved Family

## **ACKNOWLEDGEMENTS**

I would like to express my gratitude to my supervisor, Prof. Dr. Ali Kalkanlı for his guidance, advice, support, encouragement and valuable suggestions throughout the course of the studies.

I would also like to thank Prof. Dr. Ekrem Selçuk, Prof. Dr. Bilgehan Ögel, Prof. Dr. A. Tamer Özdemir due to their guidance and support.

Thanks are also to Yusuf Yıldırım, Nilüfer Özel, Serkan Yılmaz, Gürkan Görmen, Ali Osman Atik for his patience and support during laboratory studies.

Besides, thanks to my parents, for their support, encouragement, and trust in me throughout my life.

## TABLE OF CONTENTS

ABSTRACT .....	v
ÖZ .....	vii
ACKNOWLEDGEMENTS .....	x
TABLE OF CONTENTS .....	xi
LIST OF TABLES .....	xiii
LIST OF FIGURES .....	xiv
1. INTRODUCTION .....	1
2. LITERATURE SURVEY .....	3
2.1. Tool Steels .....	3
2.2. Cold Work Tool Steels .....	4
2.2.1. Group A steels .....	4
2.2.2. Group D steels .....	5
2.2.3. Group O steels .....	5
2.3. Production Route of Cold Work Tool Steels.....	5
2.4. Carbides in Cold Work Tool Steels.....	6
2.4.1. Formation of Carbides .....	6
2.4.2. Strengthening by Carbides.....	7
2.4.3. Carbides as Crack Initiation Sites.....	8
2.5. Heat Treatment of Cold Work Tool Steels.....	9
2.5.1. Austenitizing .....	9
2.5.2. Tempering .....	10
2.6. AISI DC53.....	11

2.6.1. Heat Treatment of AISI DC53 .....	13
3. EXPERIMENTAL PROCEDURE.....	17
3.1. Experimental Procedure .....	17
3.2. Retained Austenite Determination .....	21
4. RESULTS and DISCUSSIONS .....	23
4.1. Solidification Analysis of AISI DC53 Tool Steel.....	23
4.2. Microstructural Analysis of the Wedge-Shaped Castings to Reveal Cooling Rates.....	25
4.3. Simulation of Wedge Specimens .....	34
4.4. Retained Austenite Content .....	38
4.5. Carbide Size Distribution.....	39
4.6. Microstructures of Water Atomized AISI DC53 Steel .....	41
4.7. Microstructures of Thin Section Cast and Rolled AISI DC53 Steel.....	48
4.8. Austenitization of AISI DC53.....	50
4.9. Microstructure & Retained Austenite Content of Tempered Steel .....	62
4.10. Hardness.....	66
5. CONCLUSION .....	69
6. SUGGESTIONS FOR FUTURE WORK .....	71
REFERENCES .....	73
CURRICULUM VITAE.....	79

## LIST OF TABLES

### TABLES

Table 2.1 Technical datasheet of AISI DC53 [32].....	12
Table 3.1 Chemical composition of steel used (mass%).....	17
Table 4.1 Retained austenite content for different wedge sections.....	39
Table 4.2 Carbide size distribution against the section thickness in wedge specimens produced by both sand and permanent mould casting after carbide extraction .....	41

## LIST OF FIGURES

### FIGURES

Figure 2.1 Schematic illustration of a typical commercial processing route for the fabrication of tool steels and tools (EAF: electric arc furnace, LF: ladle furnace, VD: vacuum degassing, VIM: vacuum induction melting, QT: quenching and tempering [20]) .....	6
Figure 2.2 Carbides in 8%Cr-steels: specimens after (a) solidification, (b) reheating, (c) hot compression, (d) annealing, (e) quenching, and (f) tempering [20].....	7
Figure 2.3 Orowan system of carbides .....	8
Figure 2.4 Crack initiation and crack propagation of carbide [26].....	9
Figure 2.5 Hardness retained austenite and grain size as function of austenitizing temperature [32].....	14
Figure 2.6 Hardness vs. tempering temperature for AISI DC53 for different austenitizing temperatures [32].....	14
Figure 2.7 CCT diagram at 1030°C austenitizing temperature [32].....	15
Figure 3.1 Schematic diagram of casting specimen .....	18
Figure 3.2 The experimental set-up of (a) and (b) water atomization unit, (c) permanent mould casting unit.....	19
Figure 3.3 The tool steel thin slabs produced by permanent copper mould casting..	20
Figure 3.4 Heat treatment procedure of the tool steel thin slabs produced by permanent copper mould casting .....	21
Figure 4.1 Cooling curve and first derivative of AISI DC53 tool steel.....	24
Figure 4.2 XRD pattern of AISI DC53 steel specimen cast into thermal analysis cup .....	24
Figure 4.3 As-cast microstructure of the AISI DC53 alloy poured into a thermal analysis cup showing dark martensite and light austenite phases surrounded by the carbide phases .....	25

Figure 4.4 Dendritic microstructures taken from upper (thick) section of the sand mould cast wedge sample.....	27
Figure 4.5 Dendritic microstructures taken from middle section of the sand mould cast wedge sample. ....	28
Figure 4.6 Dendritic microstructures taken from tip section of the sand mould cast wedge sample. ....	29
Figure 4.7 Dendritic microstructures taken from upper (thick) section of the permanent copper mould cast wedge sample.....	30
Figure 4.8 Dendritic microstructures taken from middle section of the permanent copper mould cast wedge sample.....	31
Figure 4.9 Dendritic microstructures taken from tip section of the permanent copper mould cast wedge sample.....	32
Figure 4.10 SDAS versus section thicknesses measured on the sand and copper permanent mould cast specimens.....	33
Figure 4.11 Variation in the cooling rate versus the section thickness of as-cast tool steel solidified in sand and copper moulds .....	34
Figure 4.12 Cooling curves of 6 thermocouples placed at cross section of sand mould sample .....	36
Figure 4.13 Cooling curves of 5 thermocouples placed at cross section of copper mould sample .....	36
Figure 4.14 Cooling rate and temperature distribution of each region of sand mould sample obtained from Novacast program: (a) cooling rate, (b) temperature distribution .....	37
Figure 4.15 Cooling rate and temperature distribution of each region of copper mould sample obtained from Novacast program: (a) cooling rate, (b) temperature distribution .....	37
Figure 4.16 Niyama shrinkage amount of wedge specimens (a) sand mold, (b) copper mold .....	38
Figure 4.17 Carbide extracted from tip section of the tool steel cast in copper mould. The average carbide size of the tip region is 7-8 $\mu\text{m}$ . ....	40

Figure 4.18 Microstructure of water atomized AISI DC53 tool steel powder obtained by SEM.....	43
Figure 4.19 Dendritic microstructure of as-atomized powder particle.....	43
Figure 4.20. Refined equiaxed microstructure of as-atomized powder particle.....	44
Figure 4.21 Dendritic and refined equiaxed microstructure of as-atomized powder particle .....	44
Figure 4.22 X-ray diffractogram of water atomized powder sample obtained by Cu K $\alpha$ radiation.....	45
Figure 4.23 EDS analyses of primary carbide .....	46
Figure 4.24 EDS analyses of primary carbide and metastable austenite .....	47
Figure 4.25 Sieve analyses result of AISI DC53 tool steel powder produced by water atomization (particle size vs. percentage of particles).....	47
Figure 4.26 Sieve analyses result of AISI DC53 tool steel powder produced by water atomization (% percent retained vs. particle size) .....	48
Figure 4.27 As- cast microstructure of tool steel produced by permanent copper mould casting. ....	49
Figure 4.28 As-rolled microstructure of tool steel produced by permanent copper mould casting.....	49
Figure 4.29 M <sub>7</sub> C <sub>3</sub> primary carbide structure of (a) as-cast and (b) as-rolled tool steel slabs produced by permanent copper mould casting. ....	50
Figure 4.30 Microstructure of commercial steel austenitized at 1000°C.....	52
Figure 4.31 Microstructure of commercial steel austenitized at 1025°C.....	52
Figure 4.32 Microstructure of commercial steel austenitized at 1050°C.....	53
Figure 4.33 Microstructure of commercial steel austenitized at 1075°C.....	53
Figure 4.34 Microstructure of commercial steel austenitized at 1100°C.....	54
Figure 4.35 Microstructure of commercial steel austenitized at 1125°C.....	54
Figure 4.36 Microstructure of commercial steel austenitized at 1150°C.....	55
Figure 4.37 Microstructure of commercial steel austenitized at 1175°C.....	55
Figure 4.38 Microstructure of developed steel austenitized at 1000°C .....	56
Figure 4.39 Microstructure of developed steel austenitized at 1025°C .....	56



Figure 4.40 Microstructure of developed steel austenitized at 1050°C.....	57
Figure 4.41 Microstructure of developed steel austenitized at 1075°C.....	57
Figure 4.42 Microstructure of developed steel austenitized at 1100°C.....	58
Figure 4.43 Microstructure of developed steel austenitized at 1125°C.....	58
Figure 4.44 Microstructure of developed steel austenitized at 1150°C.....	59
Figure 4.45 Microstructure of developed steel austenitized at 1175°C.....	59
Figure 4.46 XRD patterns of commercial steel at different temperatures for 1 hour	60
Figure 4.47 XRD patterns of austenitized new steel at different temperatures for 1 hour	60
Figure 4.48 Retained austenite amount of new steel and commercial one after austenitizing heat treatments .....	61
Figure 4.49 Hardness values of new steel and commercial one after austenitizing heat treatments. ....	61
Figure 4.50 Microstructure of commercial steel austenitized at 1025°C for 1 hour and tempered twice at 525°C for 30 minutes .....	62
Figure 4.51 Microstructure of commercial steel austenitized at 1025°C for 1 hour and tempered twice at 525°C for 60 minutes .....	63
Figure 4.52 Microstructure of commercial steel austenitized at 1025°C for 1 hour and tempered twice at 525°C for 90 minutes .....	63
Figure 4.53 Microstructure of commercial steel austenitized at 1025°C for 1 hour and tempered twice at 525°C for 120 minutes .....	64
Figure 4.54 Microstructure of developed steel austenitized at 1025°C for 1 hour and tempered twice at 525°C for 30 minutes .....	64
Figure 4.55 Microstructure of developed steel austenitized at 1025°C for 1 hour and tempered twice at 525°C for 60 minutes .....	65
Figure 4.56 Microstructure of developed steel austenitized at 1025°C for 1 hour and tempered twice at 525°C for 90 minutes .....	65
Figure 4.57 Microstructure of developed steel austenitized at 1025°C for 1 hour and tempered twice at 525°C for 120 minutes .....	66

Figure 4.58 The hardness values of the tool steel (new steel) developed and commercial one after tempering heat treatments..... 67





## CHAPTER 1

### INTRODUCTION

High-chromium cold work tool steels are employed for cold work applications involving surface temperatures of not more than 200°C, such as coining and punching [1]. In this temperature range, the steels must have high hardness, high wear resistance and toughness and high dimensional stability during hardening and tempering. Conventional production methods involving thick section casting of cold work tool steels result in low solidification rates. Low solidification rates cause segregation of alloying elements, and large and coarse interdendritic primary carbide structures after solidification. The main drawback of these steels is the nonhomogeneous microstructure because of the high segregation of alloying elements during solidification [2].

Once solidified, a segregated microstructure is very resistant to subsequent heat treatment (quenching and tempering) and steels with segregated microstructures have brittle fracture and anisotropic properties that are problematic [3]. Primary carbides are difficult to solutionize into the tool steel matrix by heat treatment. Conventional tool steel production techniques, such as ingot casting and subsequent alternating solutionizing and forging cycles, have been applied to dissolve and refine the primary carbides. However, it is more convenient to prevent their formation by processes having fast solidification rates.

Individual coarse carbides with irregular and rounded shapes increase the stress concentration at the matrix/carbide interface, and the carbide clusters cause microcracks in cold work tool steels, and the coalescence and growth of these microcracks cause brittle failure during loading of these materials. To avoid this type of brittle fracture of the tool steels, the primary  $M_7C_3$  ( $M = Cr, Mo, V$ ) carbides must

be refined, spheroidized and homogeneously distributed [4]. Therefore, the toughness of the steel can be improved. To achieve this, elemental segregation must be lowered by increasing the solidification rate.

Recently, researches relating to solidification of tool steel alloys with high solidification rate having more attention [5-7]. Compared with conventional casting techniques, fast and rapidly solidified products have finer carbides and small austenite grain size [8] and macrosegregation-free microstructures [9]. One of most popular and viable processes with high solidification rate is water atomization. Water atomization has proven to be a low-cost process to achieve fine particle size distributions for iron, high and low-alloyed steel powders. The economic advantages, prealloying capability and solubility extension of carbide forming alloying elements of water atomization provide considerable advantages over competing technologies [10]. Due to high solidification rates achieved during water atomization, formation of chunky shaped coarse primary carbides can be completely eliminated. Due to refined carbide size and more homogeneous distribution of these carbides in the tool steel produced by water atomization, homogenization heat treatment to obtain austenite phase before quenching requires less time and energy.

The aim of the present work is to evaluate the solidification behaviour of a new type of cold work steel, AISI DC53 [11], by means of computer-assisted cooling curve analysis. Then, the effect of cooling rates on the microstructure, especially the primary carbide size of these steels, can be analysed. For this purpose, a series of tool steel alloys were melted and poured into different moulds - sand and cooper wedge-shaped moulds. In this study, the effect of various solidification rates on AISI DC53 cold work steel microstructures of the steel was investigated. In addition, the effect of solidification condition on hardness of steel after heat treatment were also investigated and compared with that of commercial AISI DC53.

## CHAPTER 2

### LITERATURE SURVEY

#### 2.1. Tool Steels

Tool steels are widely used in cold work applications such as punching, cutting, shaping, stamping and cold extrusion. They are subjected to severe loads and severe wear during use. Therefore, these steels must have high strength, hardness and wear resistance. If stresses during service exceed that the microstructure can support, breakage of tool steels is inevitable.

Tool steels are generally steels with high carbon content and heat-hardened. In order to obtain a high hardness, their matrix is usually martensitic. They are generally alloyed with alloying elements such as chromium, molybdenum, vanadium and tungsten to improve their mechanical properties [12-14].

Tool steels contain a lot of carbide phases during production due to segregation and alloying elements. These carbide phases are very hard and brittle. These carbides are embedded in the matrix and provide high wear resistance to tool steels. Depending on the alloy element added, their structures and types vary. The hardness level of the steel therefore depends on the nature of the carbides present.

Tool steel must maintain long-term performance during service. Therefore, it is very important to delay the wear of tool steel. The abrasion resistance is dependent on too many factors. Some of those;

- The amount of carbide in the structure,
- Hardness value after heat treatment,
- The type of friction between the tool and the workpiece (dry or wet),

- Distribution, hardness and shape of carbides

For good wear resistance, the carbides must be uniformly dispersed in the matrix. In this study, particular attention was paid to this and sudden and rapid solidification techniques were used for homogeneous and fine distribution of carbides. In addition, tool steels must have a certain level of toughness during their use. In tool steels, energy must be compensated more elastic than plastic to prevent permanent deformations. High carbon content and large amounts of brittle carbides significantly reduce toughness. Therefore, one or more tempering cycles after austenitizing heat treatment is very important in these steels [15].

## **2.2. Cold Work Tool Steels**

Cold work steels soften in high temperature applications and are therefore used in applications at temperatures below about 200°C. [16] Cold work tool steels are divided into three groups: A (air hardening steels), D (high carbon, high chromium steels) and O (oil hardening steels) [16]. The main alloying elements differ for each group. In general, the total alloy content is less than high temperature resistant steels [17]. Cold work tool steels have high dimensional stability and do not change their shape during quenching heat treatment [19].

### **2.2.1. Group A steels**

Group A steels contain sufficient alloying elements to achieve full hardness during quenching with air. A hardness level of 59-60 HRC can easily be achieved in thicknesses of 100-120 mm [17]. Group A steels have (very) high dimensional stability during quenching and their carbide distributions are homogeneous. The main alloying elements are carbon, molybdenum, chromium and manganese. While those with high chromium content have high resistance to softening at high temperatures, species with high manganese content can harden at temperatures lower than 110°C [18]. Group A steels are generally very suitable for high precision applications.



### **2.2.2. Group D steels**

The basic alloying elements in group D steels are carbon and chromium, 1.5-2.35% by weight and 4-12% by weight, respectively. They provide excellent wear resistance and matrix contain large amounts of carbide. Compared to group A, group D steels may be exposed to cracking during the hardening heat treatment. They are widely used in long-term moulds such as cavity, forming and deep drawing. [16], [18]. In this study, AISI DC53 steel which is a group D cold work tool steel was used. Detailed technical information of this steel is given in the following sections.

### **2.2.3. Group O steels**

Group O steels are high carbon steels which contain less basic alloying elements than other types. The hardening of steels from group O is worse than group A. Group O steels are hardened by quenching in oil. Due to the low alloying element content, only carbon (iron carbides) provides hardness and wear resistance. As a result, abrasion resistance is not as good as for group A and group D steels. The steels in this group are used for short term applications such as blanking, forming dies, gauges, pliers, etc.

## **2.3. Production Route of Cold Work Tool Steels**

The typical process route for cold work tool steels is shown in Figure 1. In the production, which is started with melting process, refining process is applied to remove impurities. Thermomechanical processes such as forging and rolling are used to refine the coarse and large carbide structure caused by segregation during solidification. Then, annealing heat treatment is conducted to obtain spherical carbide structure and soft ferritic or pearlitic matrix. The purpose of this matrix is to provide easy shaping of the product for use. Then the product is heat treated. Heat treatment is divided into two parts: austenitizing and tempering. The purpose of austenitizing is to dissolve carbides in the matrix to provide hardness and strength to the product and to convert the matrix to martensite. The purpose of tempering heat treatment is to eliminate the stresses that occur after austenitizing [20].

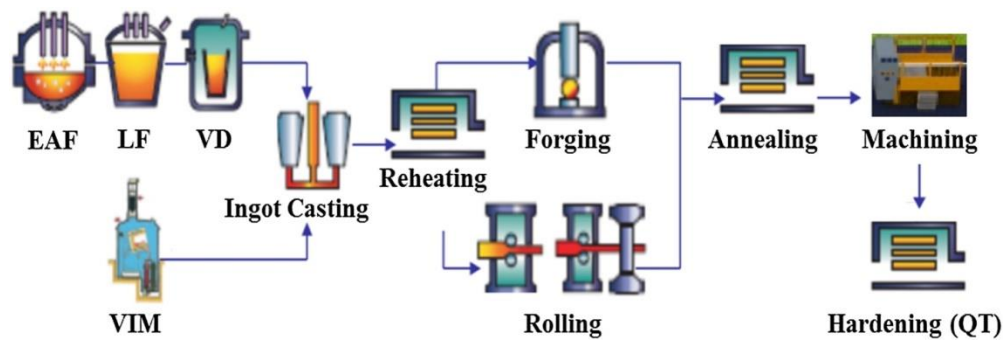


Figure 2.1 Schematic illustration of a typical commercial processing route for the fabrication of tool steels and tools (EAF: electric arc furnace, LF: ladle furnace, VD: vacuum degassing, VIM: vacuum induction melting, QT: quenching and tempering [20])

## 2.4. Carbides in Cold Work Tool Steels

### 2.4.1. Formation of Carbides

The main priority of alloying elements in cold work tool steels is to form a wear-resistant carbide structure within the matrix. Usually the atomic radii of the alloying elements are close to the atomic radius of the iron. Therefore, the alloying elements dissolve by filling the substitutional sites within the matrix. Although the atomic radius of the alloying elements is close to the atomic radius of the iron, they differ from the atomic radius of the iron. Therefore, they cause local stresses of host lattice structure in the matrix. In order to minimize this stress level, a driving force is formed for the diffusion of alloying elements into dislocation clusters and grain boundaries [21].

Diffusion of alloying elements into dislocation clusters and grain boundaries is a temperature-dependent process. It usually occurs at temperatures above 500°C. Alloy elements that diffuse into grain boundaries and dislocation clusters react with carbon atoms there, allowing the nucleation and growth of carbides [22]. Figure 2 shows the carbide structure of 8% chromium cold work tool steel at grain boundaries in various process stages during production [20].

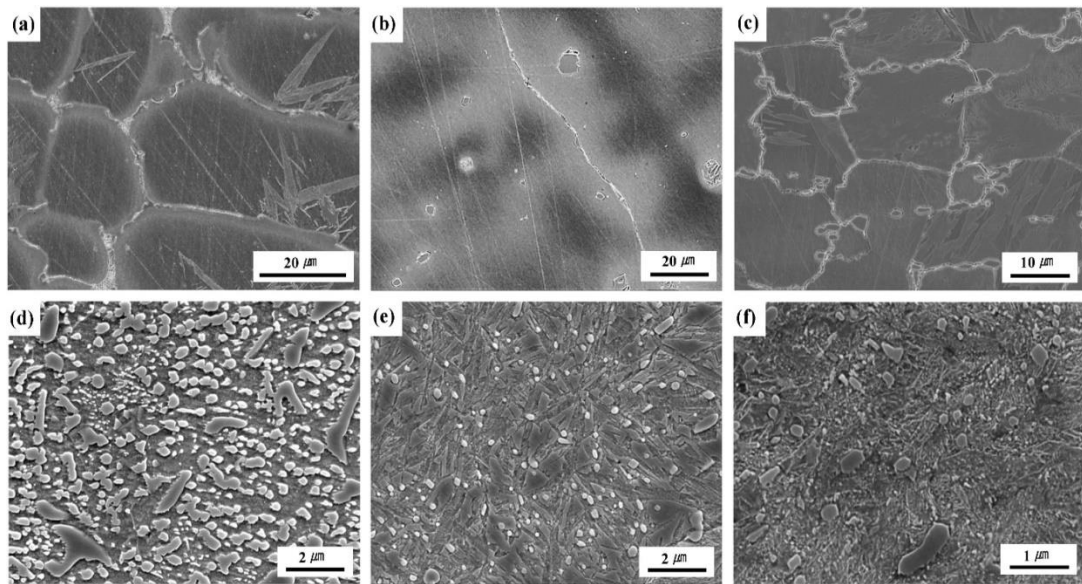


Figure 2.2 Carbides in 8%Cr-steels: specimens after (a) solidification, (b) reheating, (c) hot compression, (d) annealing, (e) quenching, and (f) tempering [20]

#### 2.4.2. Strengthening by Carbides

Carbides reinforce tool steels in two different ways.

1. In tool steels carbides are harder than matrix. Therefore, they contribute significantly to the wear resistance during service life of tool steel.
2. Carbides significantly increase the yield strength by preventing the movement of dislocations.

In cold work tool steels, carbides ranging in size from 1 to 25 $\mu\text{m}$  are resistant to wear when homogeneously distributed in the matrix [23]. In addition, carbides significantly restrict the movement of dislocations and thereby increase yield strength. The carbides randomly intersect the matrix slip planes during their growth. When a dislocation moves in the matrix slip plane, it attempts to pass through or cut around carbide. In this case, the route with the lowest resistance must be selected. By definition, the barriers are defined as strong or weak due to the high or low angles around the bending circumference of the dislocations.

Dislocations cannot surpass them when they come to carbides during their movement. They need to bend around the carbide. Usually a dislocation passes carbide through the Orowan system as shown in Figure 3. The loops formed around the carbides increase the Orowan stress which is inversely proportional to the distance between the precipitates by reducing the effective distance between the carbides [24]. Thus, the force exerted on the next dislocation that wishes to pass through the carbide is therefore increased.

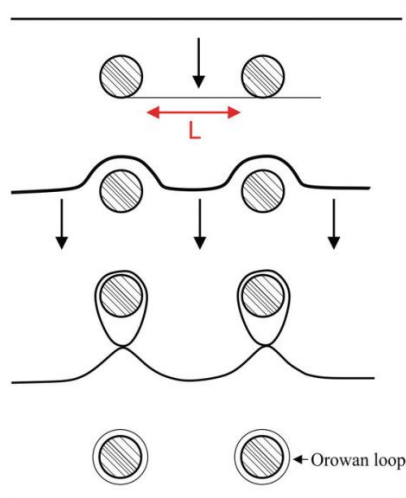


*Figure 2.3 Orowan system of carbides*

### **2.4.3. Carbides as Crack Initiation Sites**

Carbides are very useful because they provide high strength and wear resistance in service life of tool steel tool. Their main disadvantage is that they act as crack initiation points during loading as shown in Figure 4. Tool steels are exposed to various heats during use. Thermal expansion coefficients of carbides are different from iron matrix. Thus, the carbides act as crack starting points, especially if the matrix/carbide interface is semi-coherent or incoherent. The inconsistency between the carbides and the matrix results from their different lattice parameters.  $\alpha$  (Fe, bcc) = 0.28664 nm,  $\alpha$  ( $V_8C_7$ ) = 0.833409 nm). Alloy tool steels contain more than about 20 percent by volume of carbide after heat treatment. Especially if the cracks start on more than one carbide or

more than one carbide / matrix interface, the failure becomes very easy with the combination of these cracks [25].

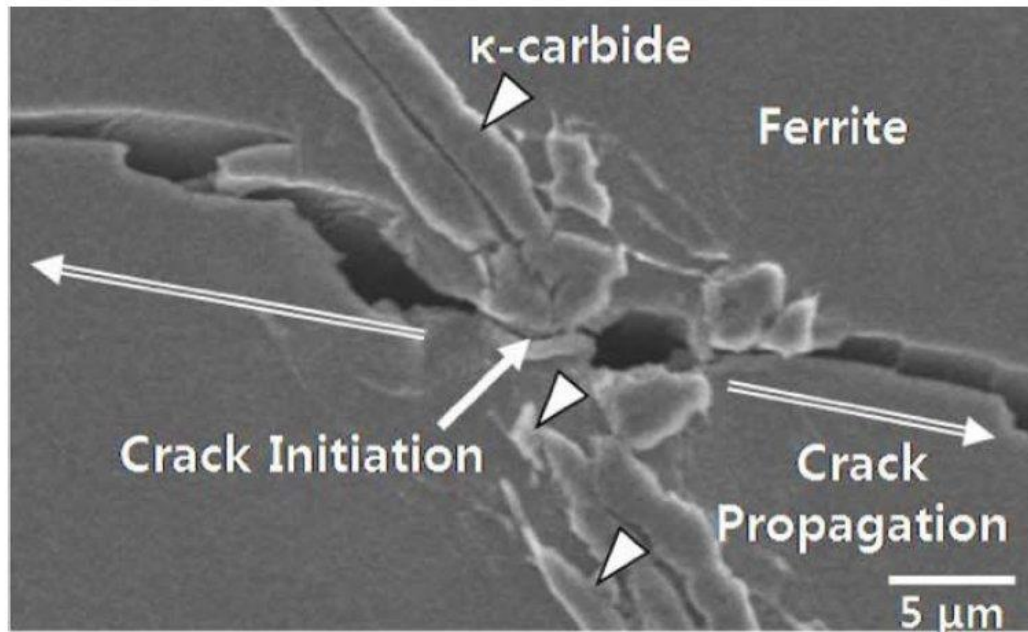


*Figure 2.4 Crack initiation and crack propagation of carbide [26]*

## **2.5. Heat Treatment of Cold Work Tool Steels**

### **2.5.1. Austenitizing**

Hardening is a heat treatment to significantly increase the hardness of the steel. Hardening heat treatment consists of two parts: austenitizing and quenching.

The austenitizing heat treatment as a single phase aims to reach the temperature at which the austenite is stable and to stand at that temperature for a certain time. In addition, generally cold work tool steels have partially stable carbides at austenite stable temperatures. Therefore, cold work tool steels are present in the carbide phase during austenitization. Choosing the correct austenitizing temperature is very important. This is because high austenitizing temperatures cause coarsening of austenite grains [27] and low austenitizing temperatures cause insoluble carbides to reduce the hardness of tool steel.

During austenitizing heat treatment, primary carbides which partially enrich the matrix in terms of alloying elements are partially soluble. Very high austenitizing temperatures are needed to completely dissolve these elements. Very high austenitizing temperatures, on the other hand, reduce the hardness considerably, as the austenite grains become coarser. In this study, rapid solidification techniques were used to obtain significantly thin primary carbides.

The dissolution of carbides enriches the matrix in terms of alloying elements. This high alloy content of austenite lowers the martensite start temperature and martensite finish temperature. In medium and high alloy cold work tool steels, martensite finish temperature is below room temperature. Therefore, a significant amount of residual austenite is present in the structure. To remove this residual austenite, one or more tempering heat treatments are applied to the steel.

### **2.5.2. Tempering**

Tempering is the final treatment of steel before use. The martensitic microstructure obtained during hardening is hard and brittle. Therefore, the basic principle of tempering is to relieve stresses during the heat treatment, increase ductility and convert residual austenite in the structure to martensite. However, it is necessary not to reduce the hardness of the steel excessively during tempering. There is a wide temperature range (i.e. 200°C to 600°C) for tempering in cold work tool steels. The temperature depends on the required properties or the application area of the tool.

During tempering, high-carbon steels also cause the precipitation of  $\epsilon$ -carbides at temperatures up to 200°C [37] and cementite ( $M_3C$ ) precipitation at temperatures between 200°C and 350°C [28]. For tool steels, temperatures between 350°C and 600°C are coarsened during tempering and the residual austenite is converted. The conversion temperature of the residual austenite depends on the steel composition.

In the range of 500°C to 600°C, very small MC and  $M_2C$  carbides of martensite structure precipitate (2-5 nm) [29,30]. These carbides are called 'annealing carbides' and have a Nano structure. The formation of these annealing carbides increases the

hardness to some extent. This phenomenon is called “secondary hardening” and is usually seen at temperatures between 500°C and 525°C. Tempering temperatures in the range of 540°C to 600°C result in thick annealing carbides that contribute less to hardness.

The conversion of residual austenite usually occurs during cooling from the tempering temperature. For steels containing high amounts of residual austenite (above 15%), a single annealing process does not convert all of the residual austenite. Therefore, double or sometimes triple tempering is required for complete conversion of residual austenite. Annealing is done in a loop. Each cycle consists of heating, holding (1 or 2 hours) and cooling to ambient temperature [31].

## **2.6. AISI DC53**

AISI DC53 is a chromium-molybdenum-vanadium alloyed tool steel which is characterised by:

- Good wear resistance
- Good chipping resistance
- High compressive strength
- High hardness (>60 HRC) after high temperature tempering
- Good through-hardening properties
- Good stability in hardening
- Good resistance to tempering back
- Good machinability and grindability
- Good surface treatment properties

AISI DC53 is a new 8 % Cr-steel. Its property profile has been carefully balanced, and the result is a very versatile tool steel which overcomes the limitations of the 12% Cr steel. The machinability, grindability and hardenability are much better, and it is

easier to make small repair welds. This means that AISI DC53 is the right choice for faster toolmaking. Table 1 shows some properties of AISI DC53 [32].

*Table 2.1 Technical datasheet of AISI DC53 [32]*

Temperature	20°C (68°F)	200°C (390°F)	400°C (750°F)
Density			
kg/m <sup>3</sup>	7730	7680	7620
lbs/in <sup>3</sup>	0.279	0.277	0.275
Modulus of elasticity			
MPa	205000	190000	180000
ksi	297000	276000	261000
Coefficient of thermal expansion			
- After low temperature tempering (60 HRC)			
per °C from 20°C	-	12.7*10 <sup>-6</sup>	-
per °F from 68 °F	-	7.1*10 <sup>-6</sup>	-
- After high temperature tempering			
per °C from 20°C	-	11.6*10 <sup>-6</sup>	12.4*10 <sup>-6</sup>
per °F from 68 °F	-	6.4*10 <sup>-6</sup>	6.9*10 <sup>-6</sup>
Thermal conductivity			
W/m*°C	-	20	25
Btu in/(ft <sup>2</sup> h °F)	-	140	170
Specific heat capacity			
J/kg °C	460	-	-
Btu/lb. °F	0.11	-	-



### **2.6.1. Heat Treatment of AISI DC53**

Prior to processing, the AISI DC53 is heated to 850°C to give the required softness and cooled to 650°C at a rate of 10°C per hour. It can be cooled in air after 650°C. After processing, AISI DC53 650°C is kept for 2 hours to relieve stresses. It is then cooled slowly to 500°C. The austenitizing temperature is between 950°C and 1080°C. However, generally between 1030°C and 1050°C is preferred. Pre-heating between 600°C - 650°C and 850°C - 900°C should be applied during austenitization. In order to prevent oxidation of the part during austenitization, austenitization should be performed in a vacuum environment. Compressed air is often used for quenching. Figure 5 shows hardness, retained austenite and grain size as function of austenitizing temperature [32]. For maximum dimensional stability and ductility, the AISI DC53 should be tempered at about 540°C and three times. Tempering at a temperature less than 540°C may increase the stiffness and compressive strength to some extent, but may also degrade crack strength and dimensional stability. When tempering twice, the minimum holding time at the temperature is 2 hours. When tempering three times, the minimum holding time is 1 hour. Figure 6 and 7 shows hardness vs. tempering temperature for AISI DC53 for different austenitizing temperatures and CCT diagram at 1030°C austenitizing temperature, respectively.

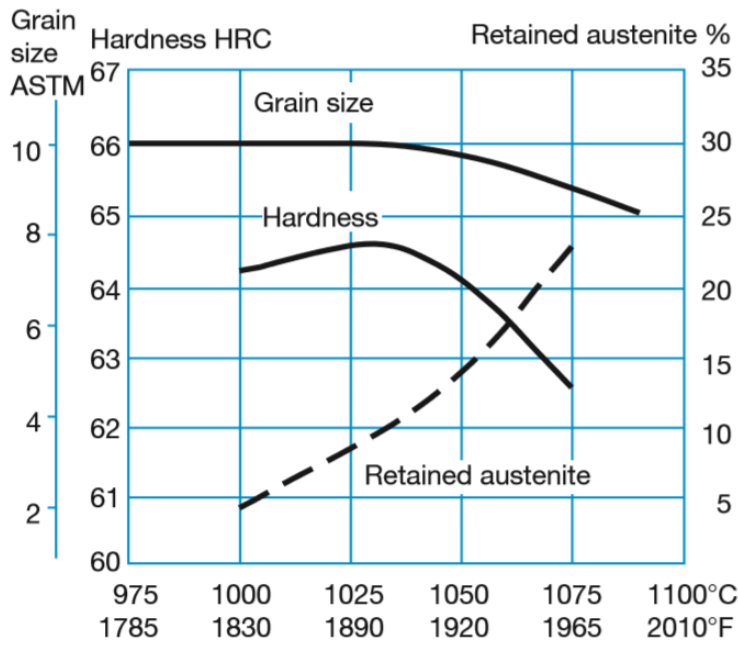


Figure 2.5 Hardness retained austenite and grain size as function of austenitizing temperature [32].

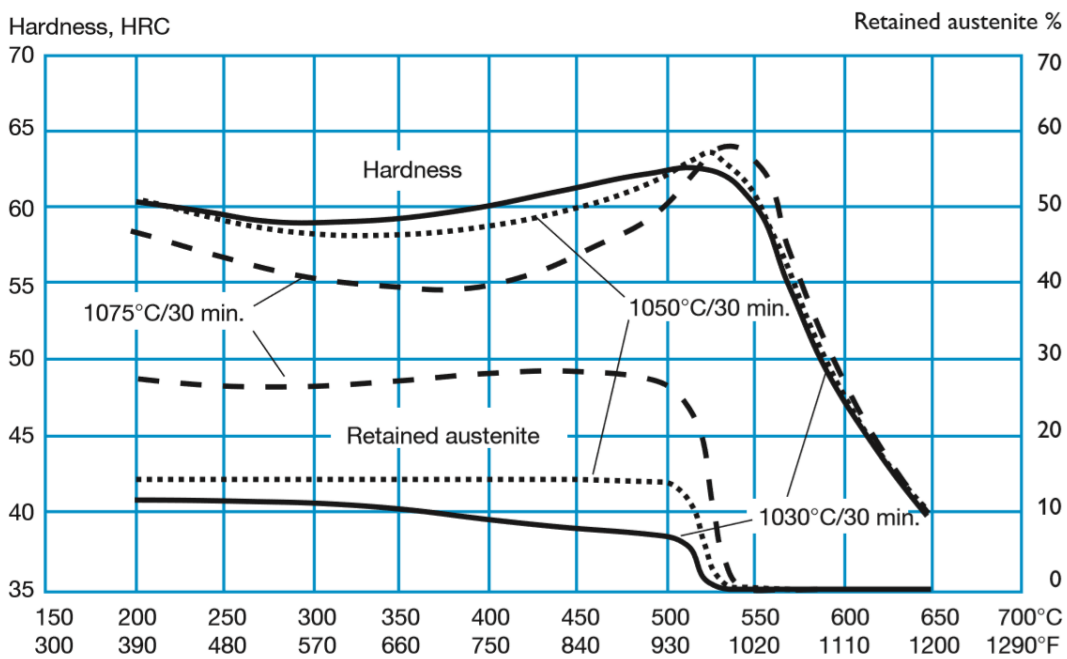


Figure 2.6 Hardness vs. tempering temperature for AISI DC53 for different austenitizing temperatures [32].

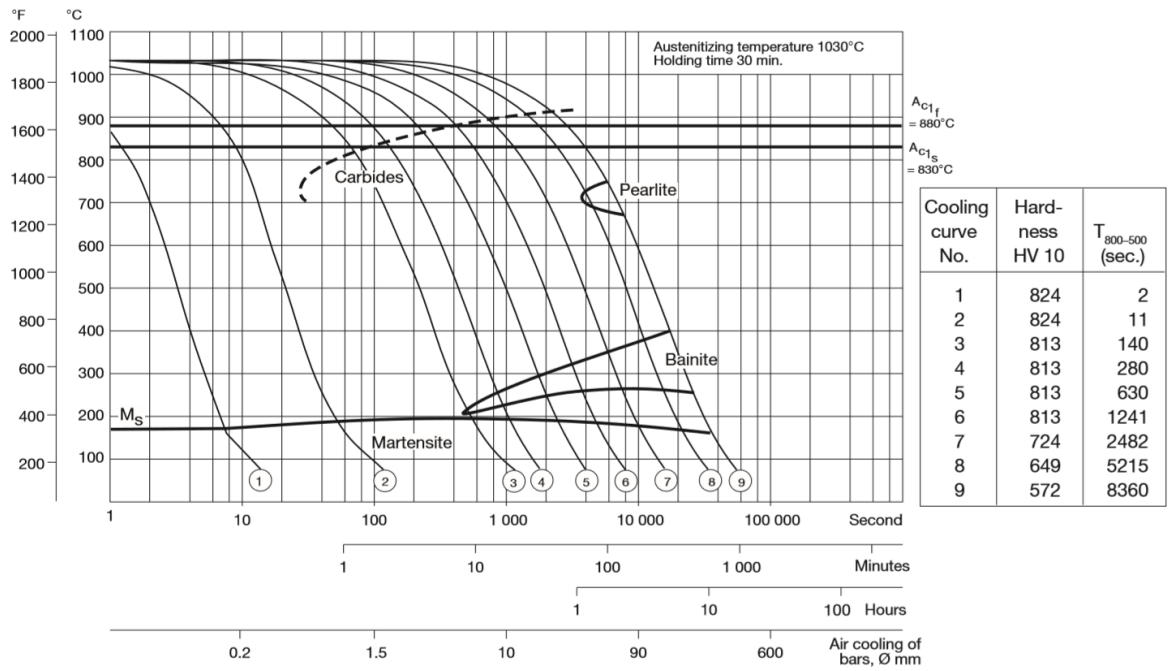


Figure 2.7 CCT diagram at 1030°C austenitizing temperature [32].



## CHAPTER 3

### EXPERIMENTAL PROCEDURE

#### 3.1. Experimental Procedure

In the first part, the chemical composition of the AISI DC53 tool steel mentioned in Table 2 was melted in induction furnace under air atmosphere.

*Table 3.1 Chemical composition of steel used (mass%)*

C	Cr	Mn	Si	Mo	V	Fe
0.894	7.863	0.482	0.913	2.467	0.486	Bal.

During the experiments, the temperature of the molten metal was controlled to a maximum of 1600°C to prevent overheating of the molten metal. Ferrosilicon powder (Fe75%Si) for 0.2% of total charge was used as deoxidizer during melting process. AISI DC53 was poured into a thermal analysis cup with an “s” type (Pt-10%Rh) thermocouple in the middle of cup at a temperature of 1550°C to perform a thermal analysis of the tool steel. Thermal analysis cup was connected to Elimko E680 thermal analysis device. Temperature data were taken from the device every second with the help of a computer. These data were processed with MATLAB 2008 program and the first derivatives were taken. In addition to this, 1cm \* 1cm \* 1cm sample was taken from the thermal analysis cup close to the hot junction of the thermocouple of the thermal analysis cup. This sample was etched with Vilella’s reagent after the necessary metallography processes was done. Microstructural examinations of sample were carried out by X-ray diffraction and optical microscopy. XRD analysis of the sample was performed with Rigaku XRD device using Cu K<sub>α</sub> radiation at 40 kV and 30 mA with a step size of 0.02° at a scanning rate of 0.02°/min.

In addition, the molten metal was poured into moulds in the form of sand and copper wedge shaped samples at 1550°C to determine the solidification behaviour of the AISI DC53 cold work tool steel at various solidification rates. To prevent possible explosions during casting, the copper wedge mould was heated to 200°C for dehumidification. The samples poured into sand and copper wedge moulds were allowed to cool to room temperature. The wedge samples were cut to obtain three cross-section samples for the upper, middle and tip regions, as shown in Figure 8.

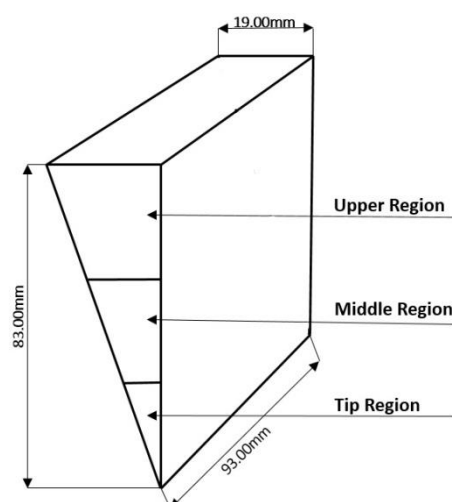


*Figure 3.1 Schematic diagram of casting specimen*

Microstructure of the samples etched with Picral were examined by scanning electron microscope. The microstructure images was enlarged and printed on A3 paper. Secondary dendrite arm spacing measurements were performed by a ruler from microstructure images printed on A3 paper. X-ray diffraction of the parts were taken with Rigaku XRD device using Cu  $K_{\alpha}$  radiation at 40 kV and 30 mA with a step size of  $0.02^{\circ}$  at a scanning rate of  $0.02^{\circ}/\text{min}$  to perform the phase analysis of the samples. The diffractogram outputs were transferred to MATLAB 2008 and the retained austenite content of the samples were calculated. Besides, carbide extraction was performed by leaching tool steel in HCl acid with 37% purity for about one week to measure the carbide size. The carbide phase obtained was purged twice with distilled water. The water-filtered carbide phase was dried at  $150^{\circ}\text{C}$  for 3 hours. The particle

sizes of the dried carbides were measured by scanning electron microscopy. Besides, three-dimensional drawing of wedge sample was made by using TRISPECTIVE drawing program. The chemical composition of AISI DC53 tool steel was introduced to the NOVACAST casting simulation program. Simulation of casting of sand and copper wedge shaped samples was performed in order to determine solidification rates of specimens.

In the second part, the melt was poured into a preheated clay bonded graphite crucible tundish at about 1000°C having a 4 mm nozzle diameter. The molten steel was atomized by four water jets with a total 200 bar pressure under the graphite crucible tundish. The experimental set-up of water atomization unit can be seen at Figure 9. The tool steel powder obtained was dried at 110°C for three hours and mounted by polyester for microstructural analysis. Microstructural examinations were done on the powder sample by scanning electron microscope. Etchant reagent used was Picral. Particle size measurement and phase analysis of powder sample were done by sieve analysis and X-ray diffraction respectively. Phase analyses of powder sample were performed by an X-ray diffractometer with Cu K $\alpha$  radiation at 40 kV and 30 mA with a step size of 0.02° at a scanning rate of 2°/min.

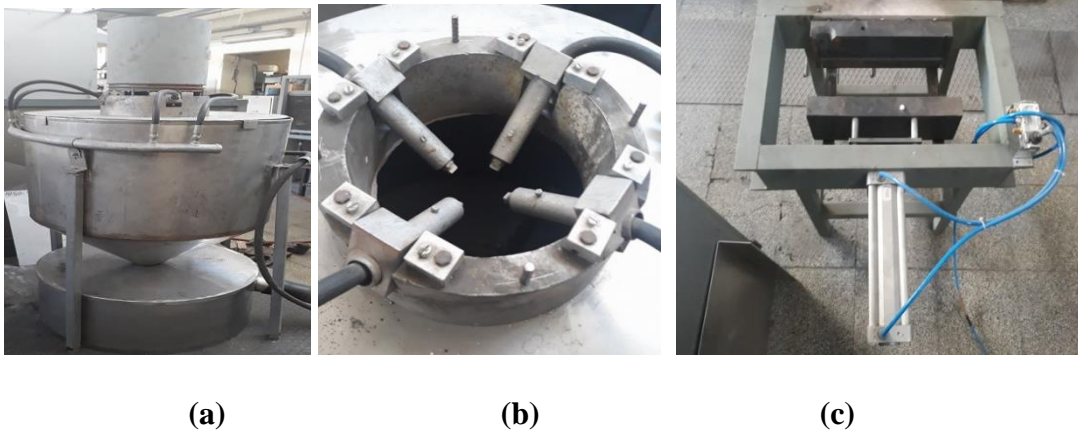


*Figure 3.2 The experimental set-up of (a) and (b) water atomization unit, (c) permanent mould casting unit.*

In the third part, the melt was poured at 1550°C in thin section copper mould. To control segregation during solidification, copper mould was heated to about 200 °C. The dimensions of as-cast slab samples were 300 mm \* 60 mm \* 8 mm. After solidification, thin slabs obtained (Figure 10) was heated to 1150°C and hold at this temperature for one hour for homogenization annealing and then hot rolling was done. During hot rolling process, about 30% reduction in thickness of slab in three steps was obtained. 10% reduction in thickness of slab was achieved in each step of rolling process.

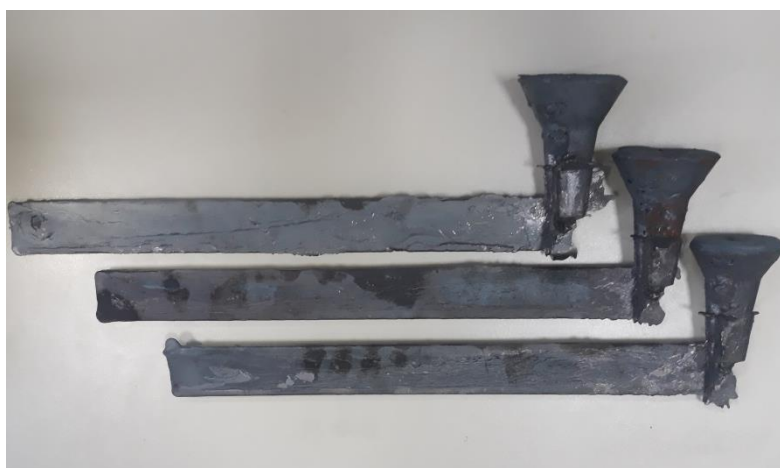


*Figure 3.3 The tool steel thin slabs produced by permanent copper mould casting*

After hot rolling, the thin slab and commercially available AISI DC53 were austenitized at 1025°C for one hour and then tempered at 525°C twice for 30, 60, 90, 120 minutes each time (figure 11). Heat treatment processes were conducted in electric furnace using heat treatment paint on each sample to prevent decarburization.

Microstructural examinations were done on all samples by optical and scanning electron microscope. Etchant reagent used is Picral for all samples. Phase analyses of samples were performed by an X-ray diffractometer. The diffractogram outputs were transferred to MATLAB 2008 and the retained austenite content of the samples were



calculated. Hardness values of heat treated cast slabs were obtained on the polished surfaces by Rockwell hardness tester in C scale with an applied load of 150 kg.

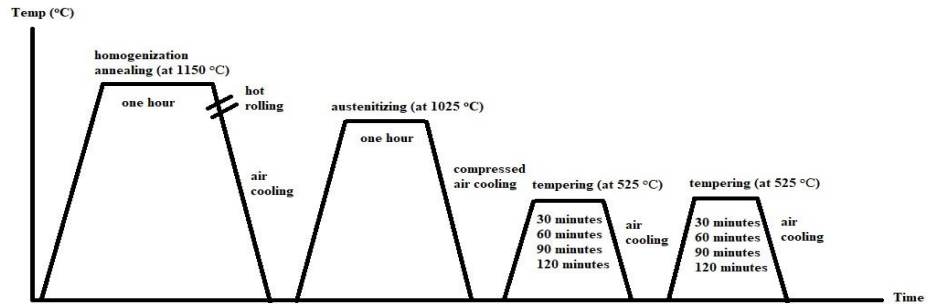


*Figure 3.4 Heat treatment procedure of the tool steel thin slabs produced by permanent copper mould casting*

### 3.2. Retained Austenite Determination

The volume fraction of the retained austenite of steel was determined by using a Rigaku X-ray diffractometer using Cu  $K_{\alpha}$  radiation based on the integrated intensity of the martensite and austenite peaks (direct comparison method) using following equation [1]:

$$I_{\text{austenite}}/I_{\text{martensite}} = \frac{R_{\text{austenite}} * C_{\text{austenite}}}{R_{\text{martensite}} * C_{\text{martensite}}}$$

Where  $I_{\text{austenite}}$  is the integrated intensity obtained at the (220) austenite peak and  $I_{\text{martensite}}$  is the integrated intensity obtained at the (200) martensite peak of the copper and sand wedge steel samples.  $R_{\text{austenite}}$ : 65.92 and  $R_{\text{martensite}}$ : 33.55 are the multiplicity factors calculated for the (220) austenite peak and (200) martensite peak, respectively.  $C_{\text{martensite}}$  and  $C_{\text{austenite}}$  are the volume fractions of the retained austenite and martensite, respectively [33]



## CHAPTER 4

### RESULTS AND DISCUSSIONS

#### 4.1. Solidification Analysis of AISI DC53 Tool Steel

The cooling curve and first derivative of cooling curve of the AISI DC53 cold work tool steel is shown in Figure 12. The first stage of solidification begins with the nucleation and growth of the austenite phase at about 1418°C (point a). Solidification ends with the formation of a 100% austenite phase. The grain boundaries, which are enriched with carbon and alloy elements due to segregation during solidification, form primary carbides in skeletal morphology. It is understood from the first derivative of the cooling curve of the primary carbides in the skeletal morphology formed at the grain boundaries. The primary carbide phase starts to nucleate and grow at the second peak (about 1148°C) after 1418°C (point b) in the first derivative curve. The final bending point (approx. 850°C) in the first derivative curve (point c) indicates the end of the carbide formation.

X-ray diffraction pattern of thermal analysis sample taken from the region near the thermocouple is shown in Figure 13. Retained austenite and bct martensite peaks are seen in the diffraction pattern. Figure 14 shows the microstructure of tool steel solidified in the thermal analysis cup. The light phase is primary retained austenite, and the dark regions are bct martensite. The interdendritic phase, which exhibits a skeletal morphology at the austenite grain boundaries saturated by carbon and chromium, is likely to be the carbide phases. XRD analysis of these carbides extracted by leaching tool steel shows that the carbides are Cr-based  $M_7C_3$  carbides.

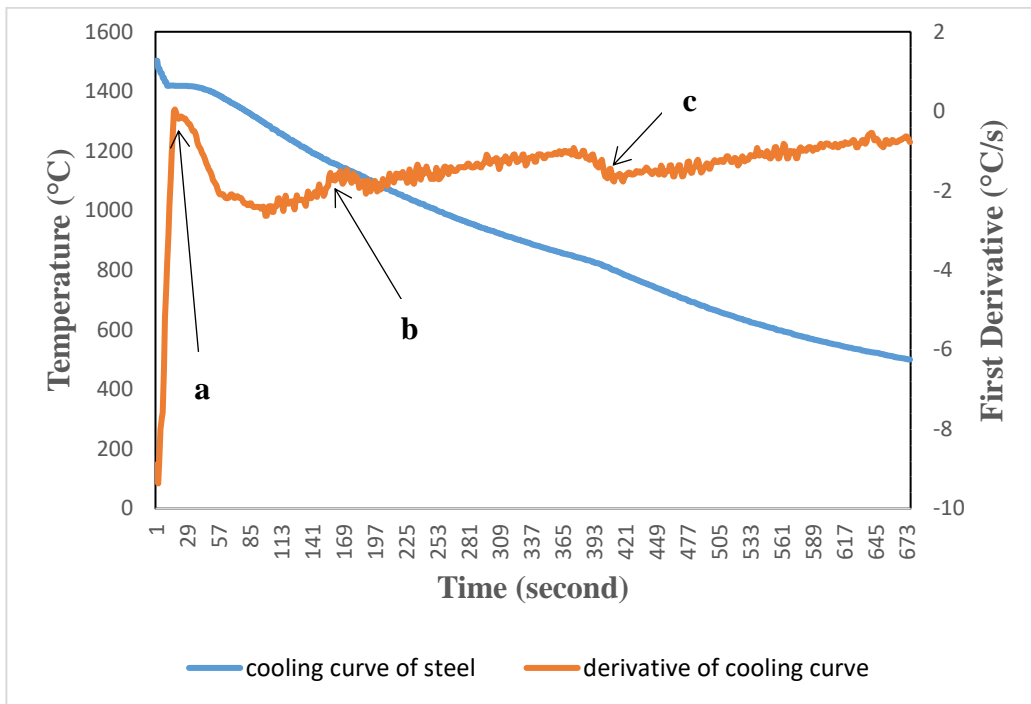


Figure 4.1 Cooling curve and first derivative of AISI DC53 tool steel

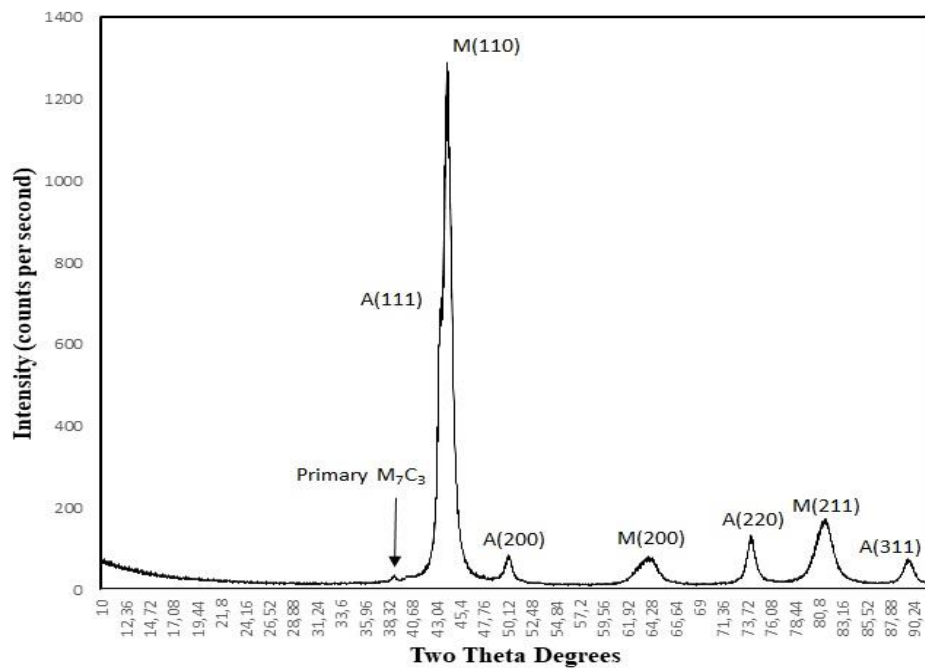
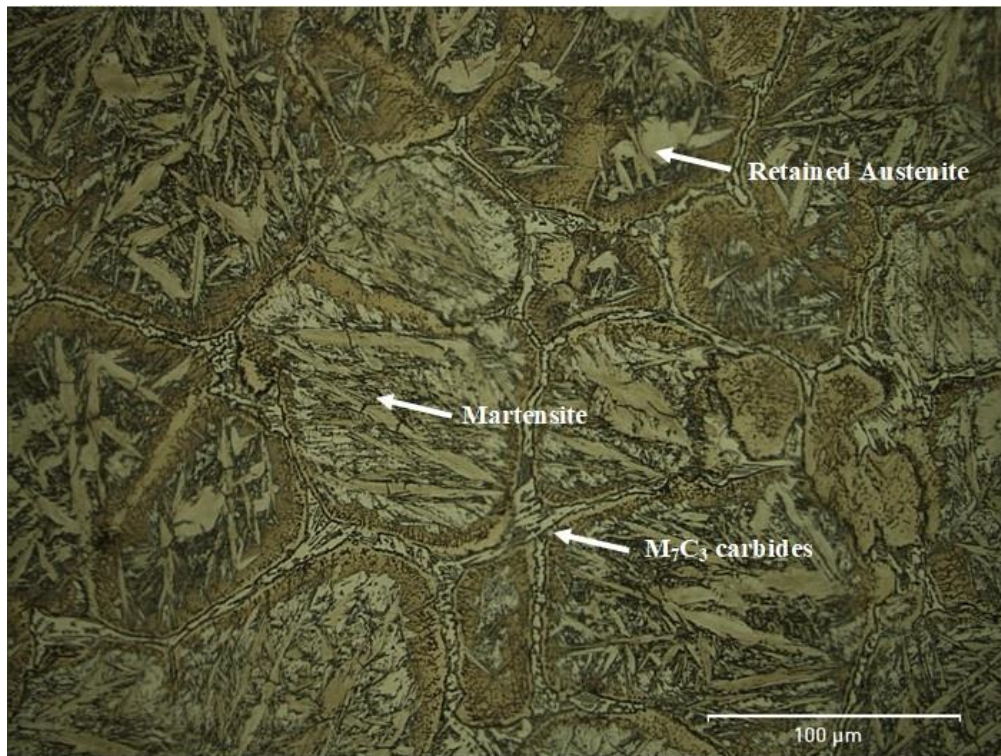


Figure 4.2 XRD pattern of AISI DC53 steel specimen cast into thermal analysis cup



*Figure 4.3 As-cast microstructure of the AISI DC53 alloy poured into a thermal analysis cup showing dark martensite and light austenite phases surrounded by the carbide phases*

#### **4.2. Microstructural Analysis of the Wedge-Shaped Castings to Reveal Cooling Rates**

The SEM microstructures of upper (thick), middle and tip sections of AISI DC53 tool steel solidified in sand mould are illustrated in Figures 15, 16 and 17, respectively. The SEM microstructures of upper (thick), middle and tip sections of AISI DC53 tool steel solidified in copper mould are illustrated in Figures 18, 19 and 20, respectively. The dendritic light grey phase is martensite and the dark regions are retained austenite. The secondary dendrite arm spacing of AISI DC53 tool steel was measured from enlarged and printed SEM images with a ruler. The largest secondary dendrite arm spacing was found in the central portion (near the top) of the sand moulded wedge specimen and the smallest secondary dendrite arm spacing was found in the tip portion of the copper moulded wedge sample. The equiaxed dendritic structure is visible in

the upper part of the sand moulded wedge sample. The secondary dendrite arm spacing (SDAS) of sand and copper moulded wedge samples showed a linear relationship to the section thickness, as shown in Figure 21. In the section thickness vs SDAS curve, the slope of the copper moulded wedge specimen ( $1.44 \times 10^{-4}$ ) is less than the slope of the wedge sample cast into the sand mould ( $2.19 \times 10^{-4}$ ).

The SDAS vs. section thickness relation was determined as follows:

- a-  $SDAS (\mu m) = 8.27 + 2.19 ST$  for sand mould casting.
- b-  $SDAS (\mu m) = 1.72 + 1.44 ST$  for copper mould casting.

Where  $ST$  = section thickness in mm.

The main reason for the difference between slopes is the low thermal conductivity of the sand with respect to copper. SDAS from wedge-shaped tool steel specimens cast into sand moulds was found to be larger than SDAS from wedge-shaped specimens cast into copper moulds with equal thickness. Because, thermal conductivity of silica sand was lower than that of pure copper. In other words, for the same cross section-thickness, the tool steel poured into the sand mould was solidified more slowly than the sample poured into the copper mould.

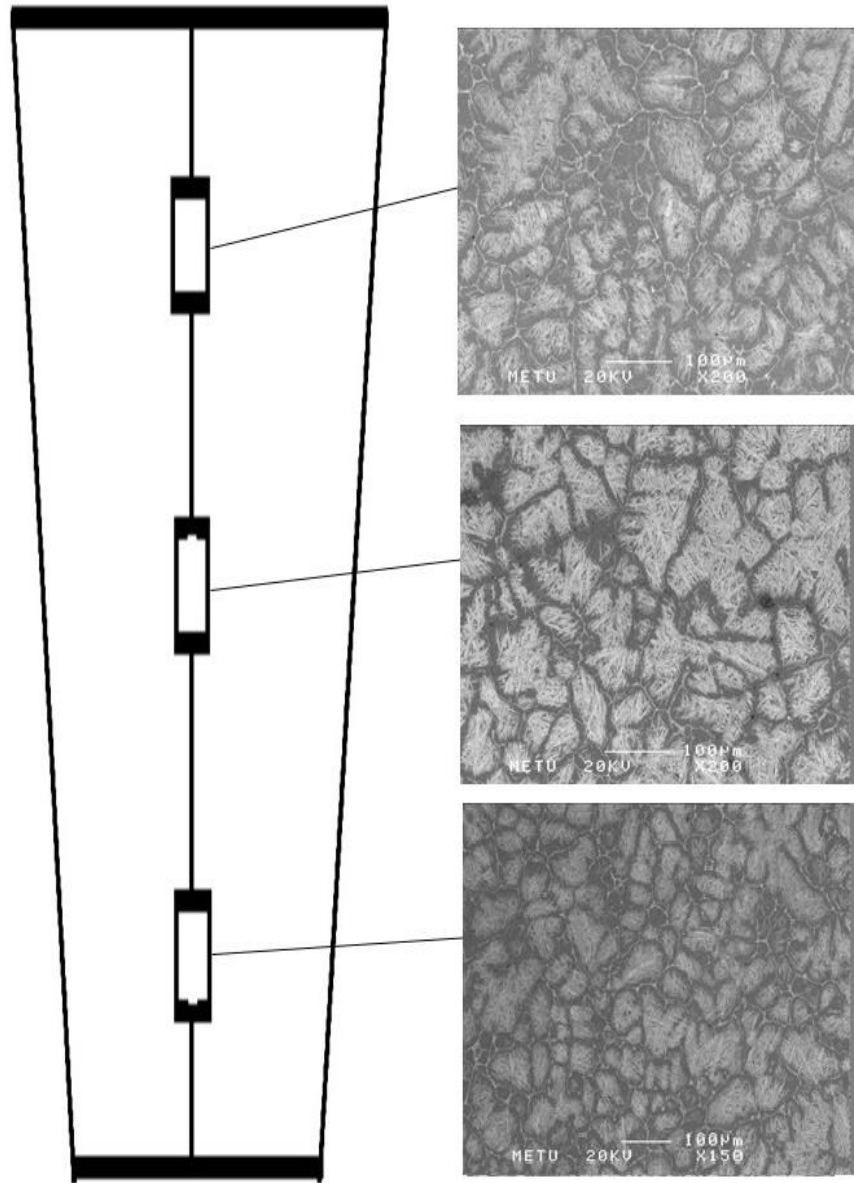


*Figure 4.4 Dendritic microstructures taken from upper (thick) section of the sand mould cast wedge sample.*

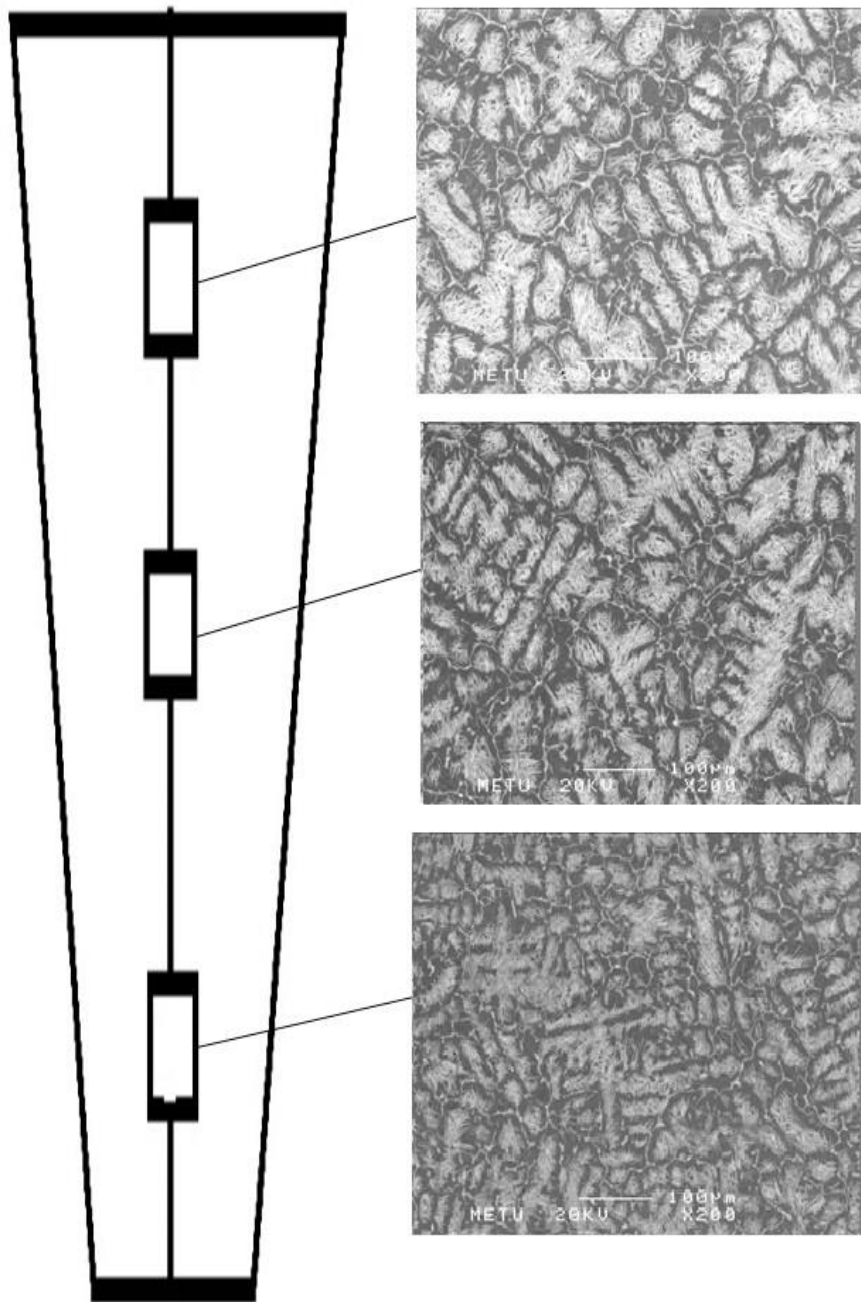


*Figure 4.5 Dendritic microstructures taken from middle section of the sand mould cast wedge sample.*



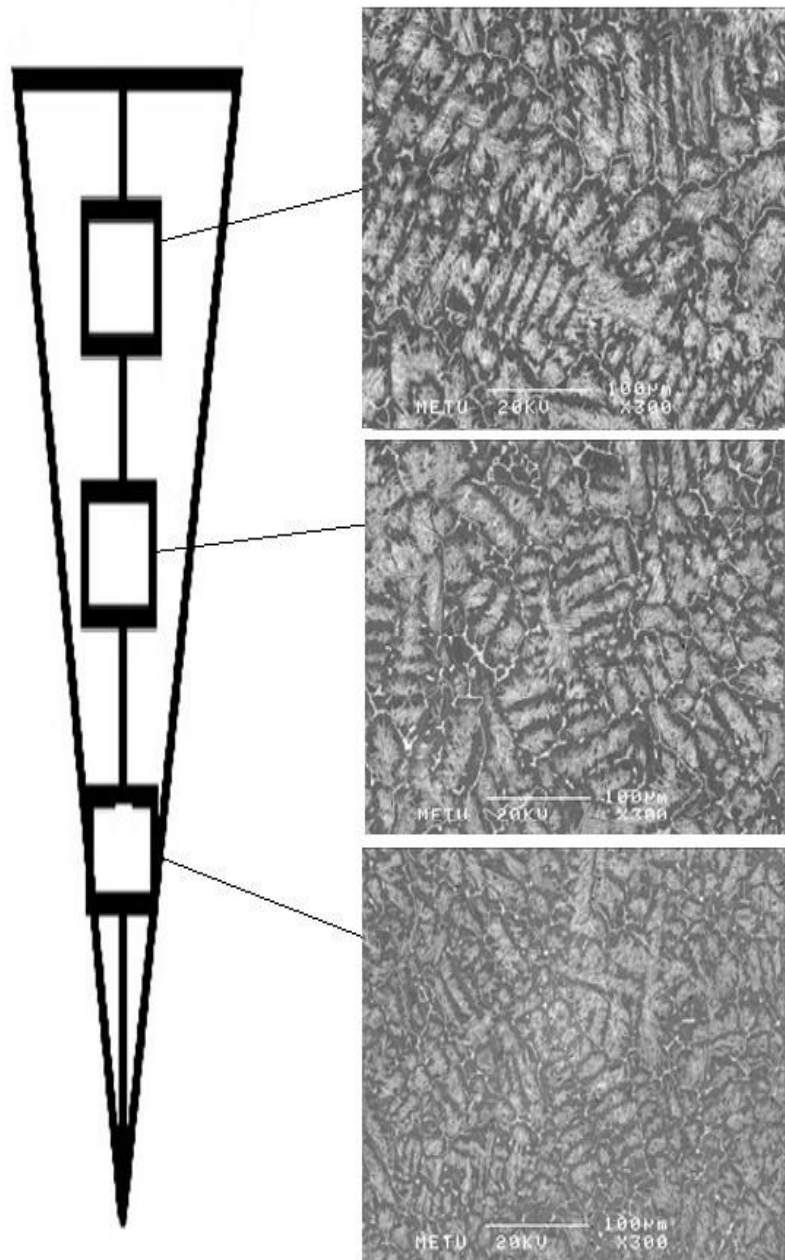


*Figure 4.6 Dendritic microstructures taken from tip section of the sand mould cast wedge sample.*

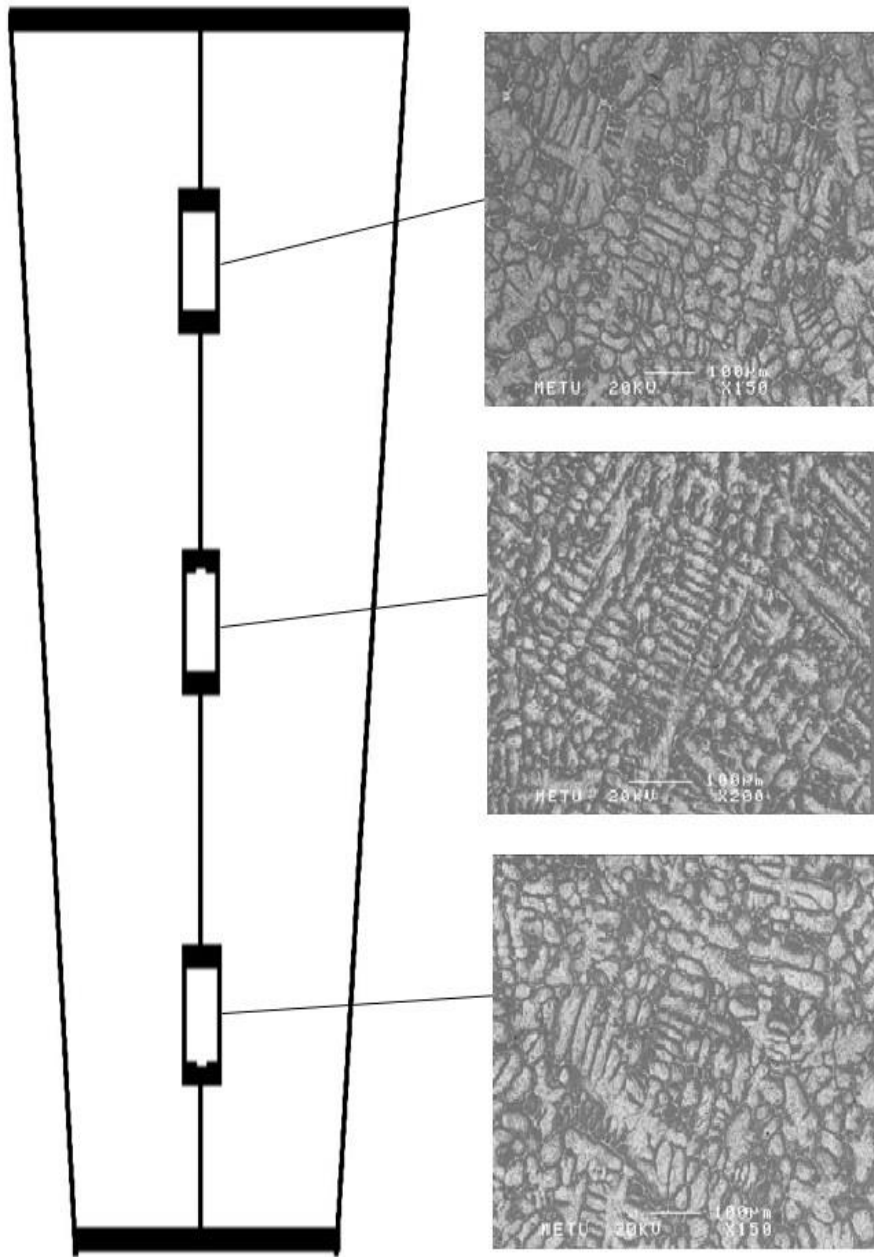


*Figure 4.7 Dendritic microstructures taken from upper (thick) section of the permanent copper mould cast wedge sample*

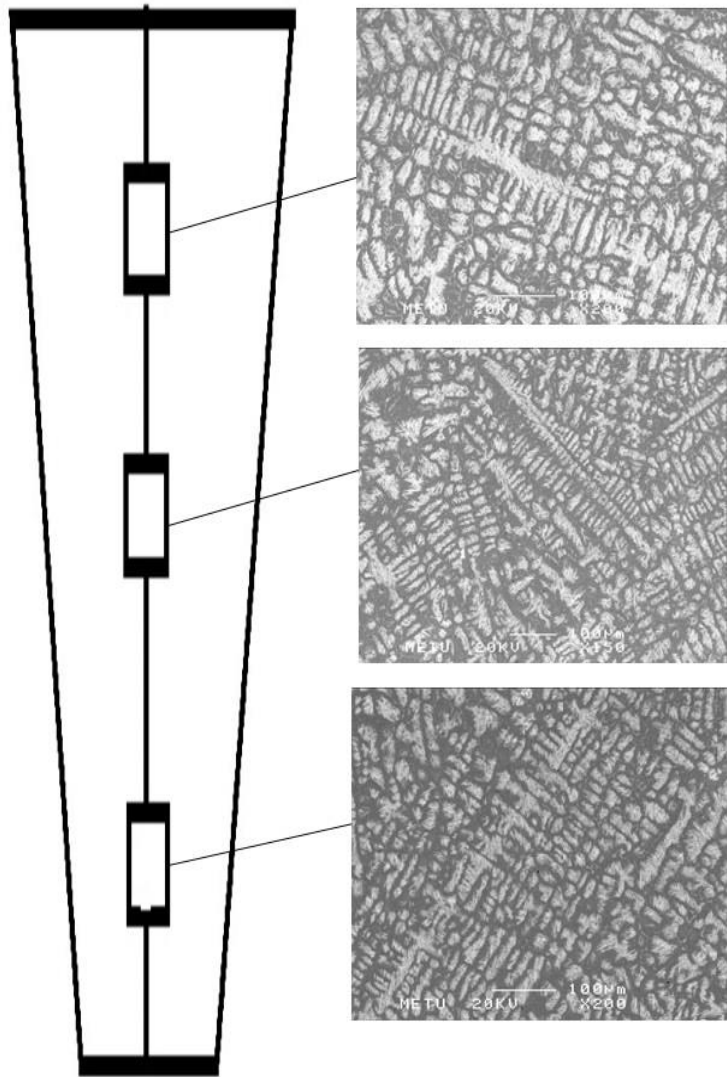


*Figure 4.8 Dendritic microstructures taken from middle section of the permanent copper mould cast wedge sample*

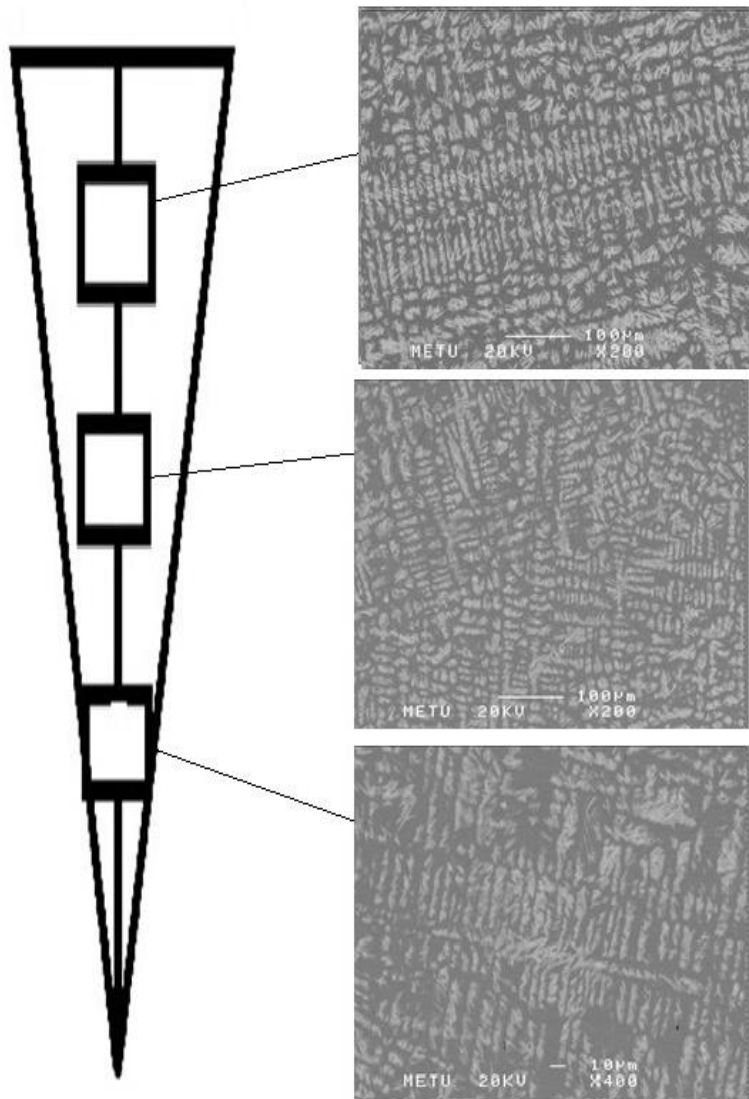


*Figure 4.9 Dendritic microstructures taken from tip section of the permanent copper mould cast wedge sample*

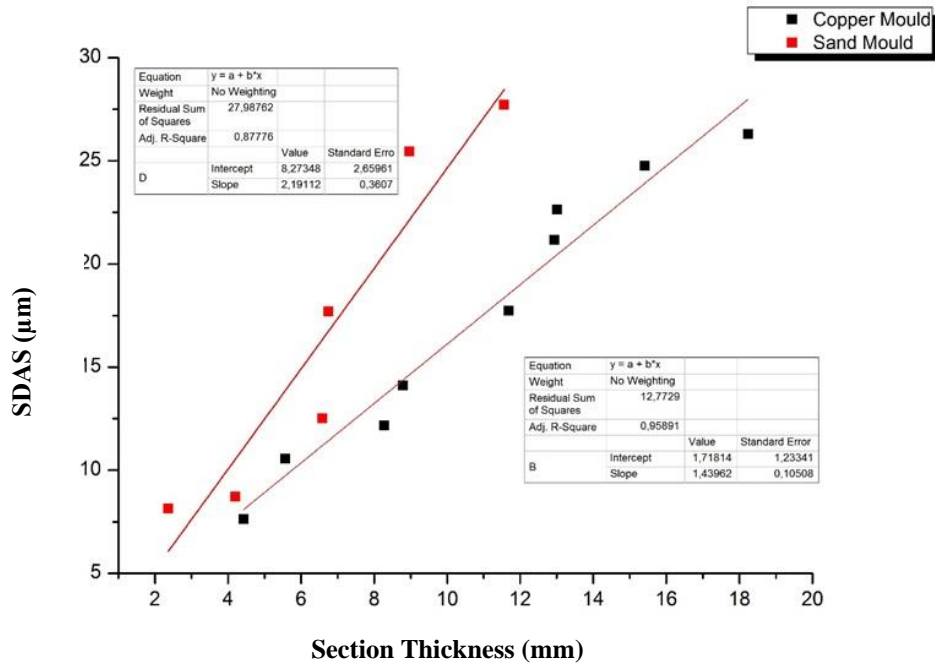


Figure 4.10 SDAS versus section thicknesses measured on the sand and copper permanent mould cast specimens

Furthermore, the cooling rates of the different parts of wedge samples solidified in the sand and copper moulds were calculated using the SDAS empirical relationship provided in Ref. [34] at distinct cooling rates ( $C_R$ ) and steel carbon contents ( $W[C]$ ):

$$SDAS = 143.9 \cdot C_R^{-0.3616} \cdot W[C]^{(0.5501 - 1.996W[C])} \quad W[C] > 0.15$$

As shown in Figure 22, the cooling rates of the sand and copper wedge samples showed an exponential relationship of roughly second order with regard to section thickness.

The cooling rate vs. section thickness relation was determined as follows:

- a- Sand casting  $CR = 1107.96 - 161.10 ST + 6.06 ST^2$
- b- Copper permanent mould casting  $CR = 7940.12 - 1092.59 ST + 37.39 ST^2$

where CR is the cooling rate.

The lowest cooling rate was found in the thick region of the middle section (close to upper section) of the sand cast wedge sample (approximately 85 °C/s), and the highest cooling rate was found in the tip region of the copper cast wedge sample (approximately 4830 °C/s).

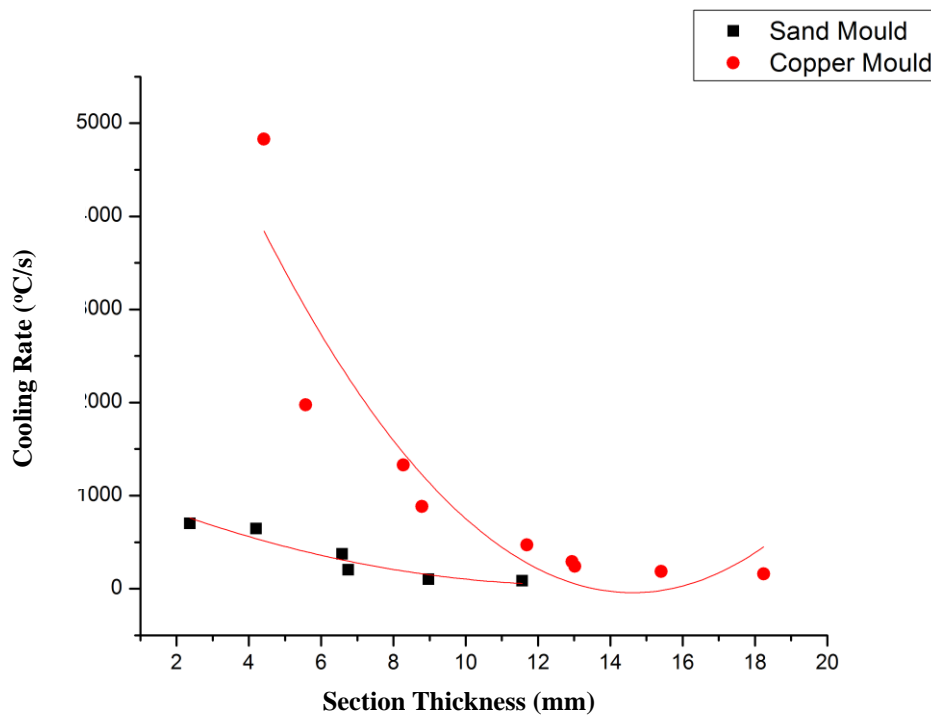


Figure 4.11 Variation in the cooling rate versus the section thickness of as-cast tool steel solidified in sand and copper moulds

### 4.3. Simulation of Wedge Specimens

Firstly, three-dimensional drawing of wedge sample was made by using TRISPECTIVE drawing program. The drawing was then opened in the NOVACAST casting simulation program. The chemical composition of AISI DC53 tool steel was introduced to the NOVACAST casting simulation program. In the program, 5 thermocouples for copper mold sample and 6 thermocouples for sand mold sample were placed in the cross-sectional area and simulation was performed. Figures 23 and 24 show the cooling curves of sand and copper mold wedge samples respectively. The

thermocouple 1 shown in Figure 23 represents the thermocouple in the tip part of the sand mold sample and the thermocouple 6 represents the thermocouple in the thickest part. The thermocouple 1 in Figure 24 represents the tip part of the copper mold sample and the thermocouple 5 represents the thickest part. As the cross-sectional thickness increases in both samples, the solidification rate decreases. As a result of the simulation, the fastest solidification rate was found to be approximately  $1.3 \times 10^3$  °C/s at the tip part of the copper mold sample. The slowest solidification rate was calculated as 1.76 °C/s in the thickest part of the sand mold sample. The value obtained by simulation ( $1.3 \times 10^3$  °C/s) were slightly different from the value calculated by using the empirical formula in the literature ( $4.83 \times 10^3$  °C/s) in section 4.2. The main reason for this is that the simulation involves the whole solidification process including boundary conditions and heat transfer coefficients, while the values calculated by the empirical formula are related to the formation of the secondary dendrite arm spacing. In other words, the empirical formula only calculated the solidification rate at the time of the formation of the secondary dendrite arm spacing. In addition, as a result of the simulation, the cooling rate and temperature distribution of each region of the sand and copper mold sample is shown in Figures 25 and 26 respectively. Figure 27 shows the graphs of the Niyama shrinkage amount obtained as a result of the simulation.

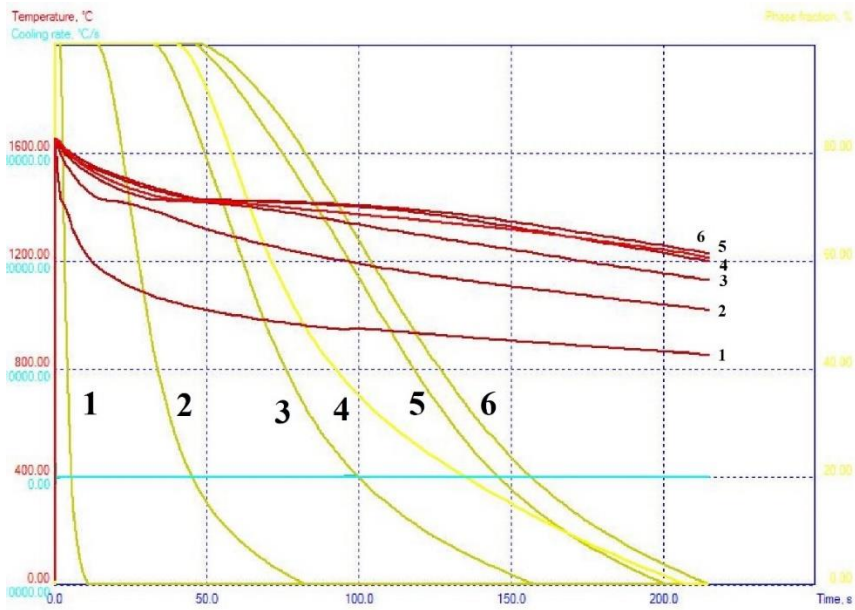


Figure 4.12 Cooling curves of 6 thermocouples placed at cross section of sand mould sample

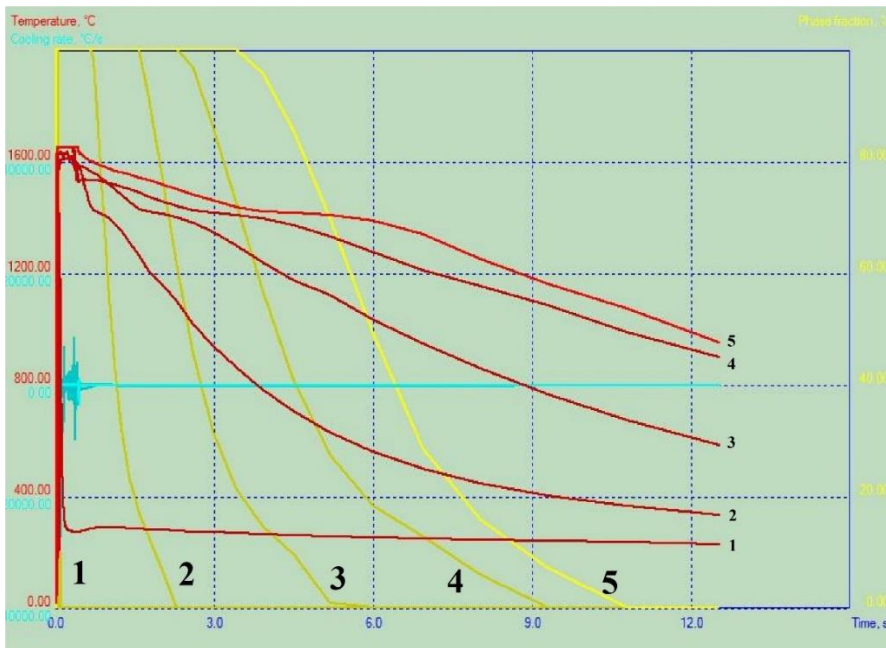


Figure 4.13 Cooling curves of 5 thermocouples placed at cross section of copper mould sample



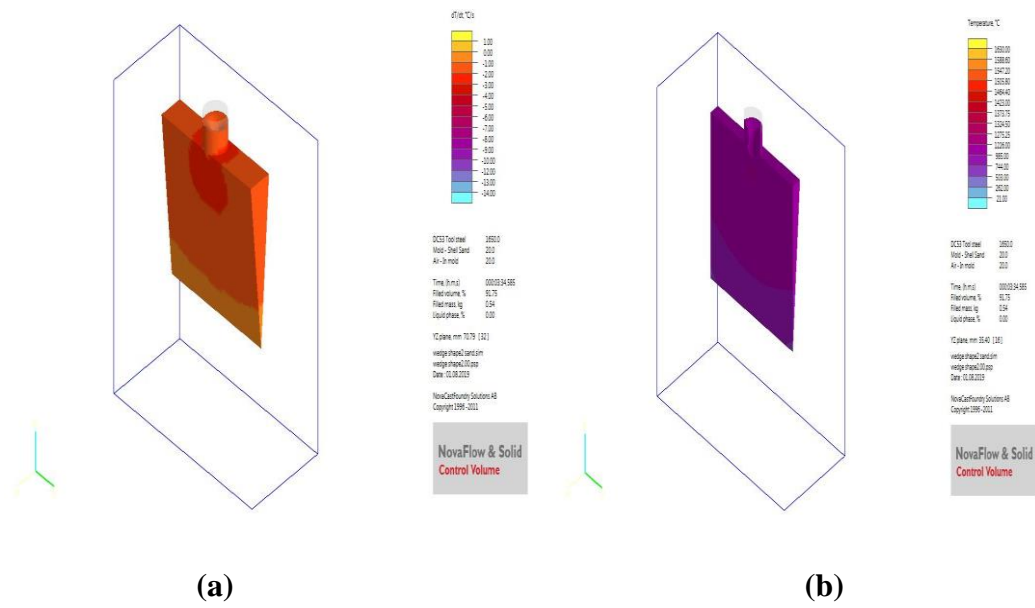


Figure 4.14 Cooling rate and temperature distribution of each region of sand mould sample obtained from Novacast program: (a) cooling rate, (b) temperature distribution

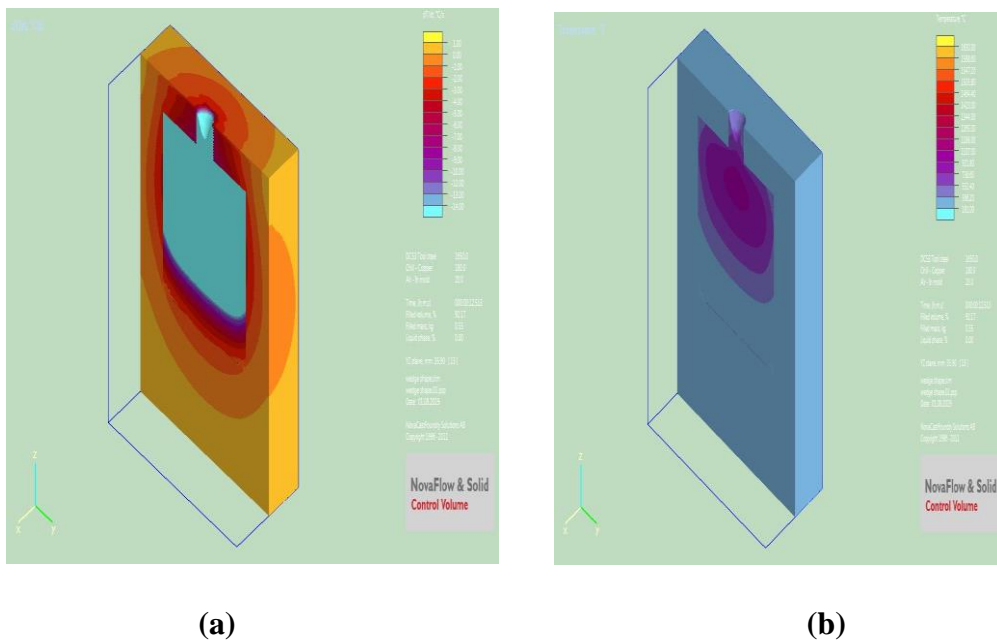


Figure 4.15 Cooling rate and temperature distribution of each region of copper mould sample obtained from Novacast program: (a) cooling rate, (b) temperature distribution

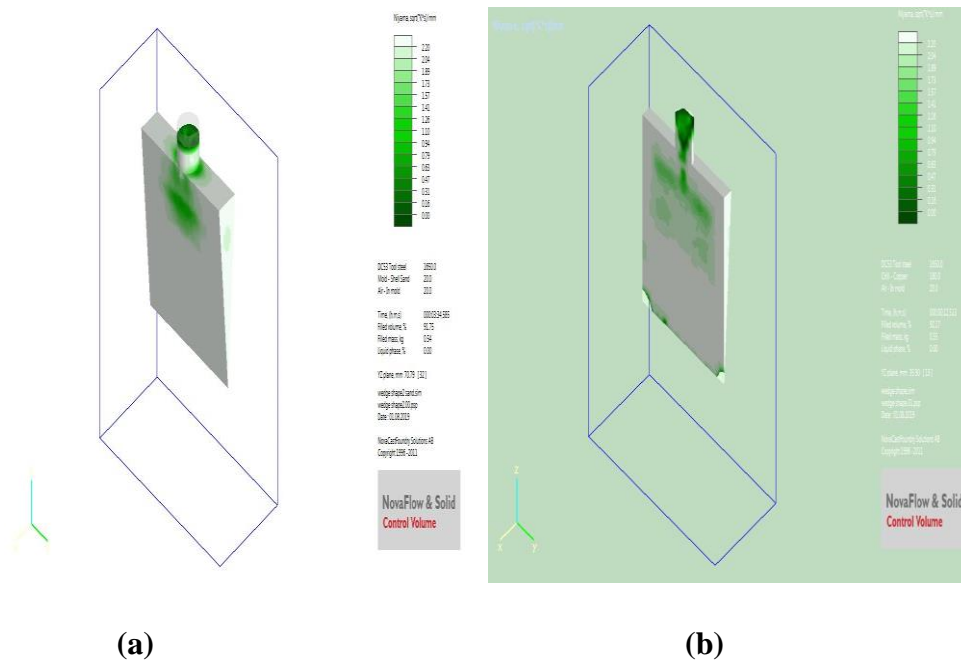


Figure 4.16 Niyama shrinkage amount of wedge specimens (a) sand mold, (b) copper mold

#### 4.4. Retained Austenite Content

In the tip and middle areas of the copper wedge steel sample, the volume fractions of retained austenite are roughly 64.26% and 39.98% percent respectively, and the volume fraction in the upper region of the copper wedge steel sample reduces to 30.72%. In the tip and middle areas of the sand wedge steel sample, the volume fraction of the retained austenite is roughly 45.43% and 27.66% respectively, and reduces to 20.88% in the upper area of the sand wedge steel sample.

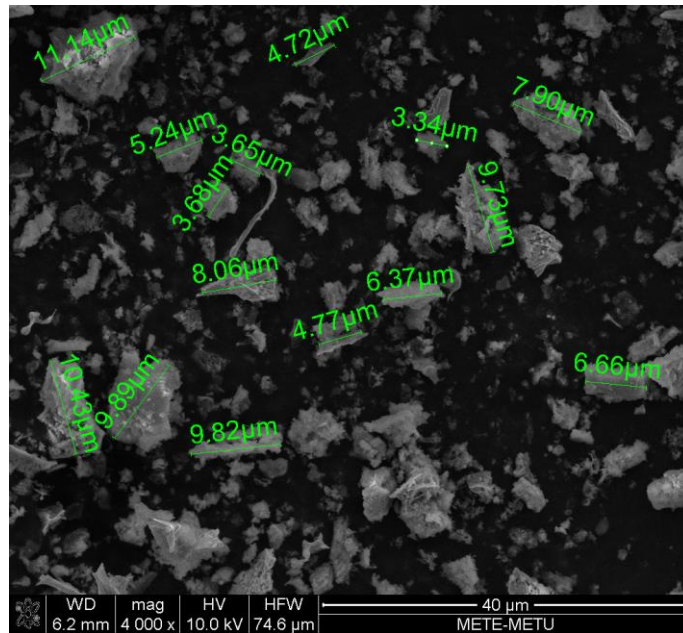
High solidification levels triggered the supersaturation of austenite with carbon and alloying elements, leading in martensite starting temperature decrease [35-37]. After solidification, there was a big quantity of metastable (or residual) austenite in the tool steel matrix of both samples at room temperature (in the range of 64.26% - 30.72% for the copper mould and 45.43% - 20.88% for the sand mould). It can also be noted that the retained austenite content rises as the solidification rate rises, as shown in Table 3.

Table 4.1 Retained austenite content for different wedge sections

Wedge Sections	Retained austenite volume percentage	
	Copper Mould	Sand Mould
Tip Region	64.26	45.43
Middle Region	39.98	27.66
Upper Region	30.72	20.88

#### 4.5. Carbide Size Distribution

The carbide size was determined from SEM images of the extracted carbides by 37% HCl acid of each region of copper and sand wedge steel samples. The carbide size of AISI DC53 tool steel in the tip and middle area for the copper wedge metal sample is roughly 7.13  $\mu\text{m}$  and 44.02  $\mu\text{m}$  respectively and increases to 97.72  $\mu\text{m}$  in the upper region. The carbide size of AISI DC53 tool steel in the tip and middle areas is about 32.16  $\mu\text{m}$  and 102.43  $\mu\text{m}$  respectively for the sand wedge steel sample and rises to 262.70  $\mu\text{m}$  in the bottom area. Figure 28 indicates the SEM picture of the extracted carbide of the tip portion taken from the sample cast into copper mould after HCl acid leaching treatment.



*Figure 4.17 Carbide extracted from tip section of the tool steel cast in copper mould. The average carbide size of the tip region is 7-8  $\mu\text{m}$ .*

The nuclei of the carbides increase in high solidification rates and the primary carbides are refined. It can be seen that the carbide size reduces in the wedge shape cast tool steel, as shown in Table 4, with an increasing solidification rate of a specific section.

*Table 4.2 Carbide size distribution against the section thickness in wedge specimens produced by both sand and permanent mould casting after carbide extraction*

Copper Wedge-shaped Mould	
Section Thickness	Average Carbide Size
4.42 – 8.27 mm (tip)	7.13 $\mu\text{m}$
8.79 – 13.02 mm (middle)	44.02 $\mu\text{m}$
13.54 – 18.24 mm (upper)	97.72 $\mu\text{m}$
Sand Wedge-shaped Mould	
Section Thickness	Average Carbide Size
2.37 – 6.58 mm (tip)	32.16 $\mu\text{m}$
6.75 – 11.56 mm (middle)	102.43 $\mu\text{m}$
11.73 – 16.07 mm (upper)	262.70 $\mu\text{m}$

#### **4.6. Microstructures of Water Atomized AISI DC53 Steel**

Figure 29 shows irregularly shaped as-atomized AISI DC53 steel powder particles, a typical feature of water atomization. The final powder particle shape generated by water atomization is quite irregular due to fast heat extraction. Compared to gas atomization, particles have less time to spheroidize [38]. Figure 30, 31 and 32 shows as-atomized powder particles' microstructures. Dendritic (Figure 30), refined equiaxed (Figure 31), and a mixture of dendritic and refined equiaxed (Figure 32) microstructures were acquired from powder particles. The formation of refined equiaxed microstructures was defined as the Karma model [39] in highly undercooled and quickly solidified specimens. According to this model, the shift from dendritic to a combination of dendritic and refined equiaxed microstructure or refined equiaxed microstructure outcome from the fragmentation of dendrites by remelting and the

formation of compound and equiaxed microstructures at the last quasi-isothermal solidification era.

Figure 33 demonstrates powder sample X-ray diffraction. The sample of powder comprises primarily of austenite and magnetite ( $\text{Fe}_3\text{O}_4$ ) phases. No martensite peak was noted in the powder sample X-ray diffraction. As several writers have stated, [40, 41] martensitic transformation is a nucleation and growth process. In this study, during the rapid solidification, the austenite dendrites are formed and high quantities of carbon and alloy elements are trapped by this phase. These elements considerably increase austenite stability. In addition, very fine grain size is another consideration in stabilizing the austenite phase because the greater nucleation barrier makes it difficult for it to convert into martensite [42]. The mixture of the above factors reduces the  $M_s$  point to a temperature below room temperature, so the martensitic transformation has not been activated. [43–45] Also, the contact of powder particles with water jets during water atomization creates particle oxidation and the powder surface contains magnetite. The magnetite phase was therefore determined by powder X-ray diffractogram.

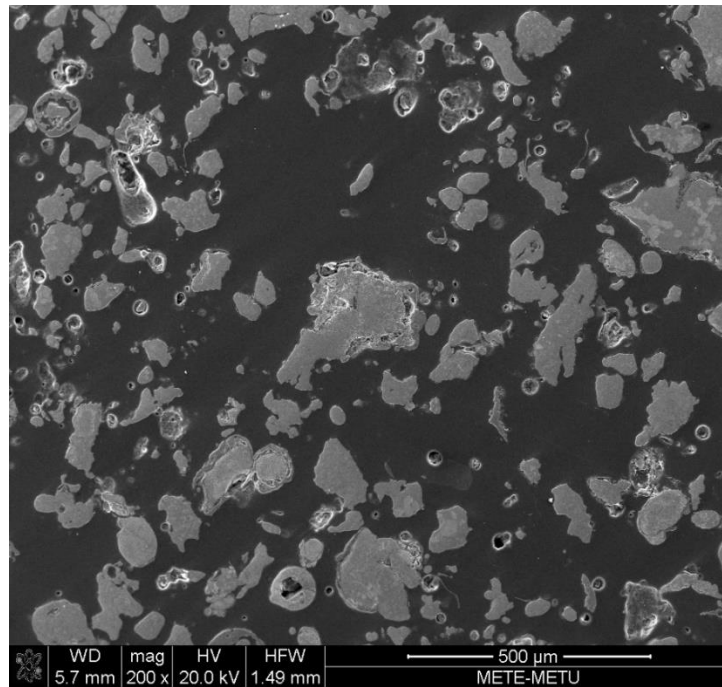


*Figure 4.18 Microstructure of water atomized AISI DC53 tool steel powder obtained by SEM*



*Figure 4.19 Dendritic microstructure of as-atomized powder particle*

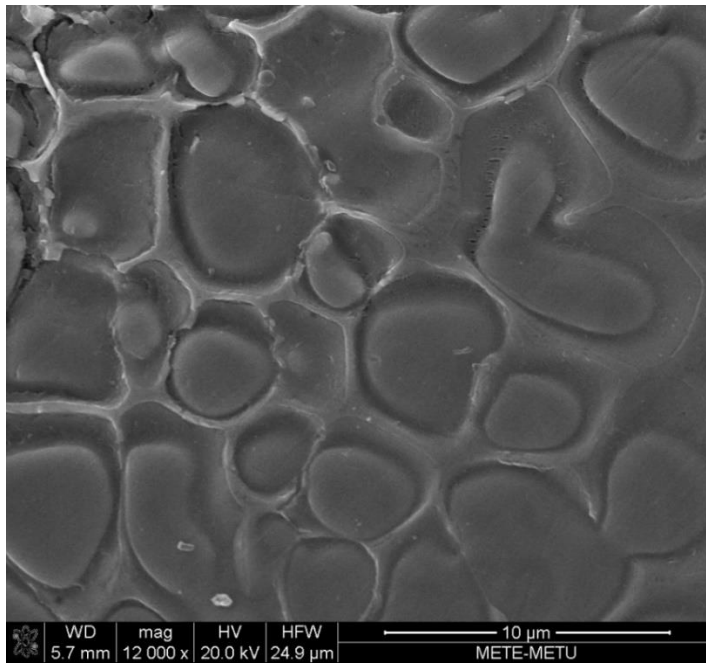


*Figure 4.20. Refined equiaxed microstructure of as-atomized powder particle*

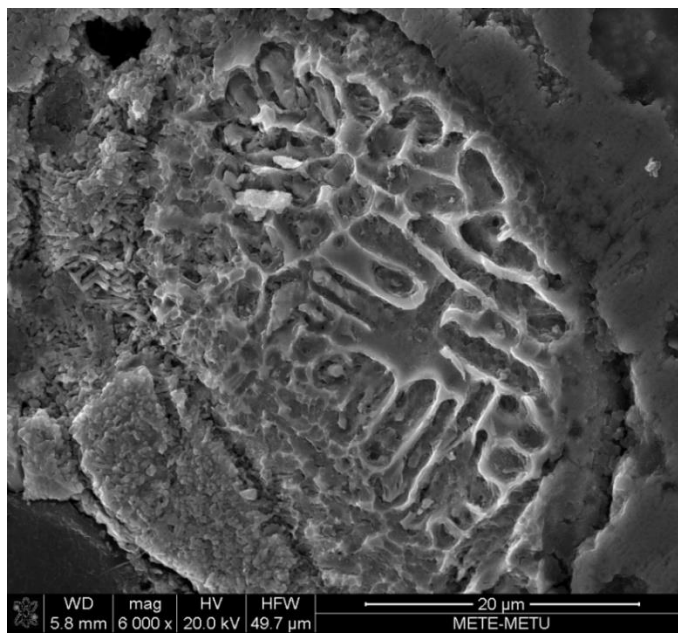


*Figure 4.21 Dendritic and refined equiaxed microstructure of as-atomized powder particle*



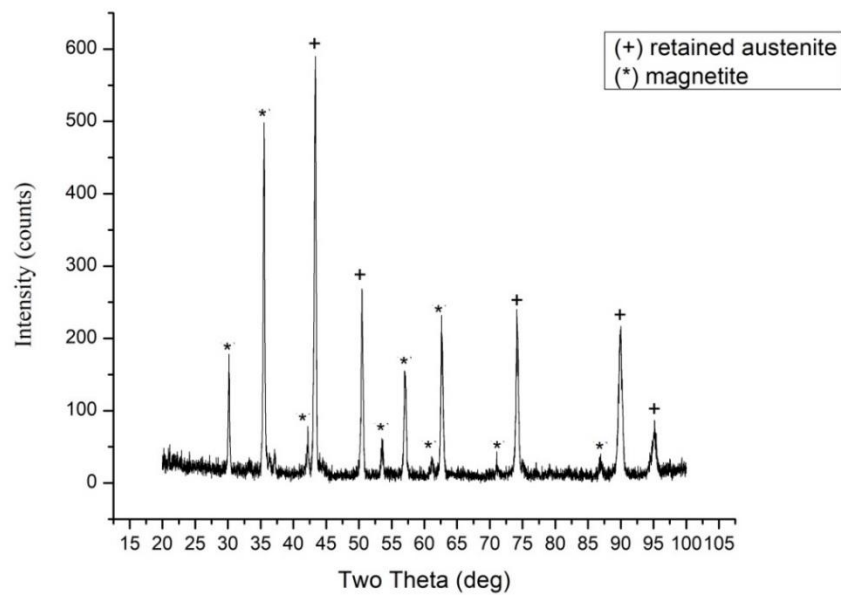


*Figure 4.22 X-ray diffractogram of water atomized powder sample obtained by Cu K $\alpha$  radiation.*

EDX analysis taken in SEM micrographs from the various grey regions (Figure 34 and 35) shows that the light grey regions contain higher amounts of alloying elements (Cr, Mo, and V). These alloying components were dismissed during the solidification process by primary austenite dendrites either between the secondary dendrite arms or at grain boundaries of equiaxed grains. Based on this compositional assessment, the light grey phase may be primary retained austenite, while  $M_7C_3$  carbides may be the dark grey phase. Fine carbide phases are either between the secondary dendrite arms or equiaxed grain boundaries in quickly solidified particles. Precipitation of carbide during solidification is the process of nucleation and growth. Carbides were refined due to the rapid solidification to not have enough time to grow. EDS analyses taken from carbides (Figure 34) and metastable austenite (Figure 35) found that primary carbides of  $M_7C_3$  contain about 7.13% atomic percentage of molybdenum which is greater than 1.75% atomic percentage of austenitic matrix molybdenum.

Approximately 52% percent of AISI DC53 steel powder particles as atomized are over 200 microns (Figure 36) and 154 microns are arithmetic mean size of water atomized tool steel particles (Figure 37).

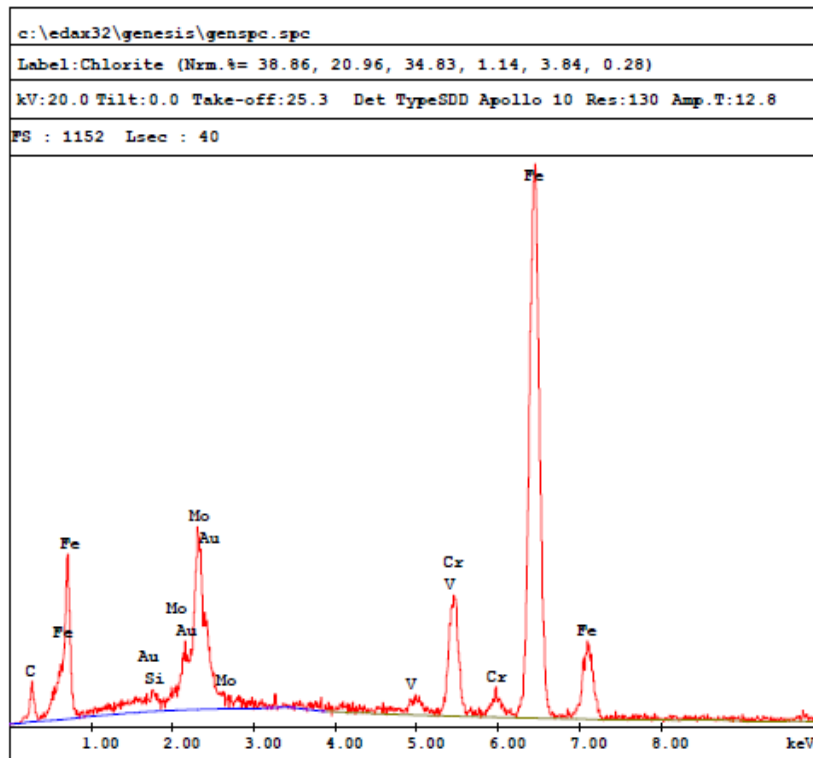


Figure 4.23 EDS analyses of primary carbide

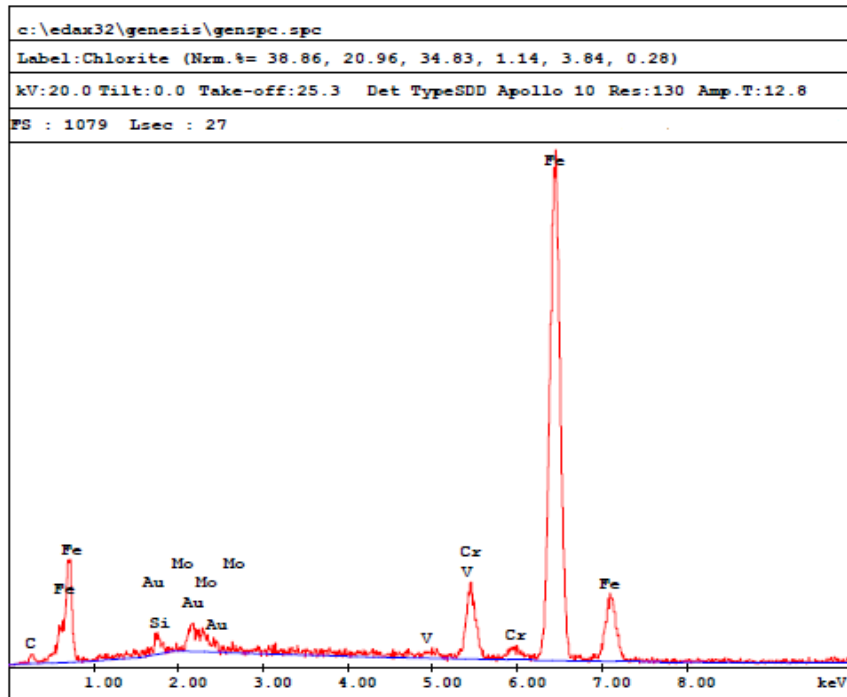


Figure 4.24 EDS analyses of primary carbide and metastable austenite

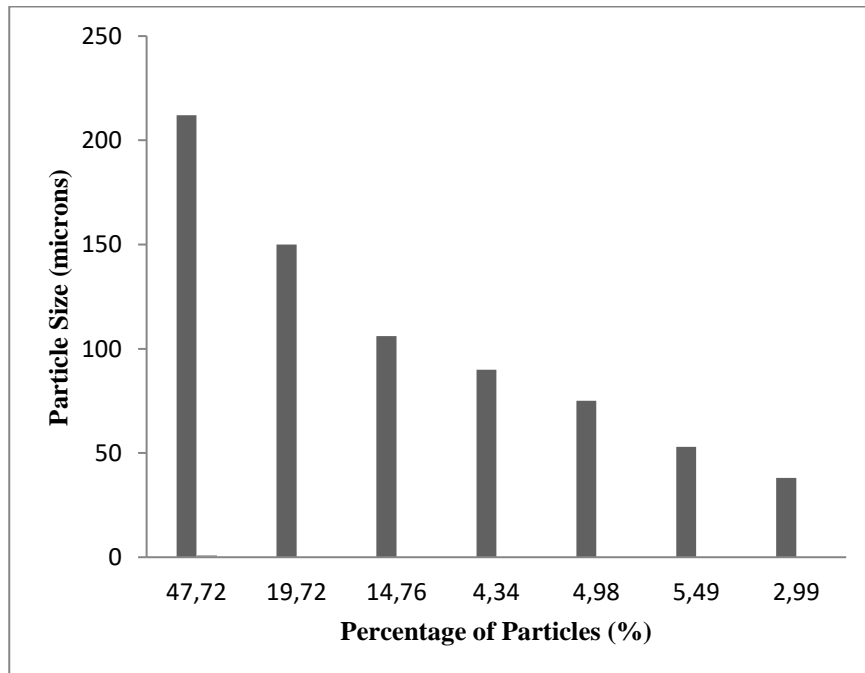


Figure 4.25 Sieve analyses result of AISI DC53 tool steel powder produced by water atomization (particle size vs. percentage of particles)

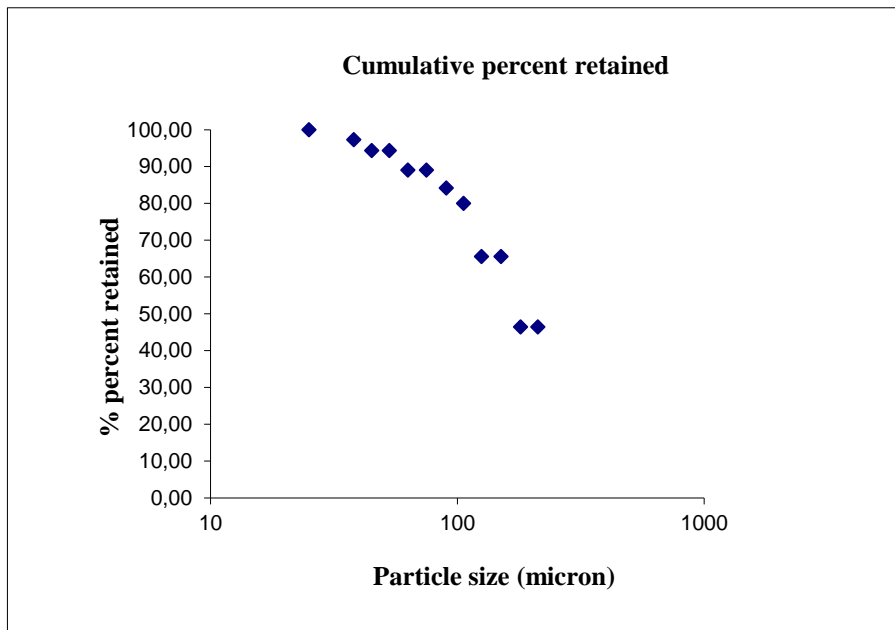


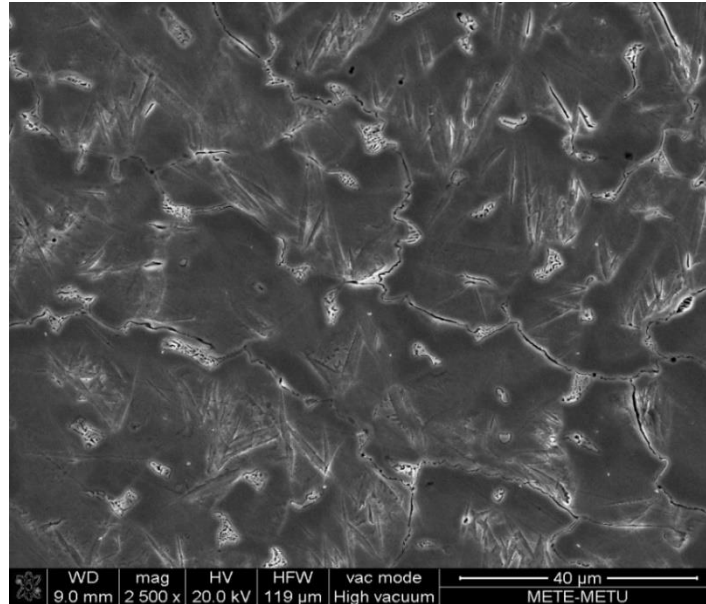
Figure 4.26 Sieve analyses result of AISI DC53 tool steel powder produced by water atomization (% percent retained vs. particle size)

#### 4.7. Microstructures of Thin Section Cast and Rolled AISI DC53 Steel

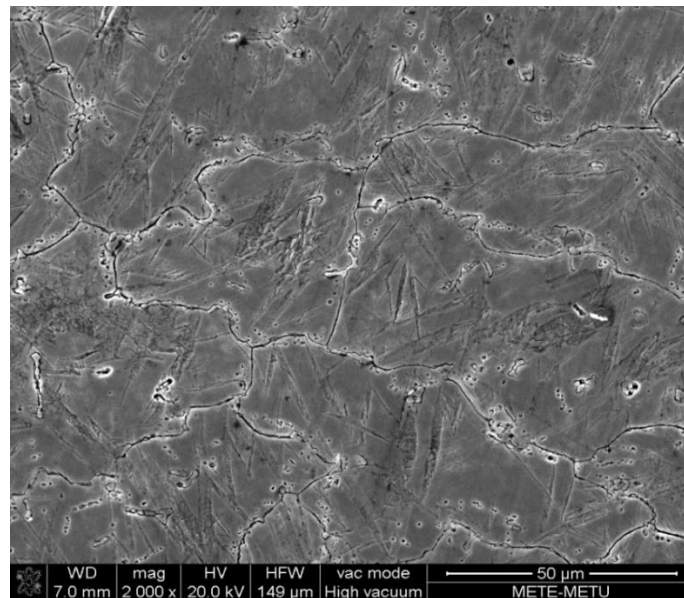
Figure 38 demonstrates as-cast microstructure of AISI DC53 with a permanent copper die cast. Dark grey areas are austenite, martensite phase is light grey areas, and  $M_7C_3$  carbides are white regions. Unlike the rapid solidification of water atomization, in the microstructure only equiaxed grains are seen. The austenite phase nucleated during fast solidification and started to grow first. Unlike rapid solidification, a certain amount of segregation occurred during the AISI DC53 steel's fast solidification process. This segregation has resulted to over-saturation with carbon and alloy elements in some areas. In these areas, owing to the drop in  $M_s$  Temperature, the retained austenite is stable at room temperature. Other region's martensitic conversion occurred, and carbide precipitation occurred at the grain boundaries. But not being able to expand along the grain boundaries and time to grow, these carbides were refined due to the fast solidification.

Figure 39 demonstrates as-rolled tool steel microstructure. Usually  $M_7C_3$  primary carbides at grain boundaries have lamellar morphology after fast solidification. Figure

40a shows this. Homogenization heat treatment at 1150°C for one hour and subsequent rolling changes in the lamellar structure of  $M_7C_3$  carbides at the grain boundaries to the plate – like shape as seen at Figure 40b



*Figure 4.27 As- cast microstructure of tool steel produced by permanent copper mould casting.*



*Figure 4.28 As-rolled microstructure of tool steel produced by permanent copper mould casting.*

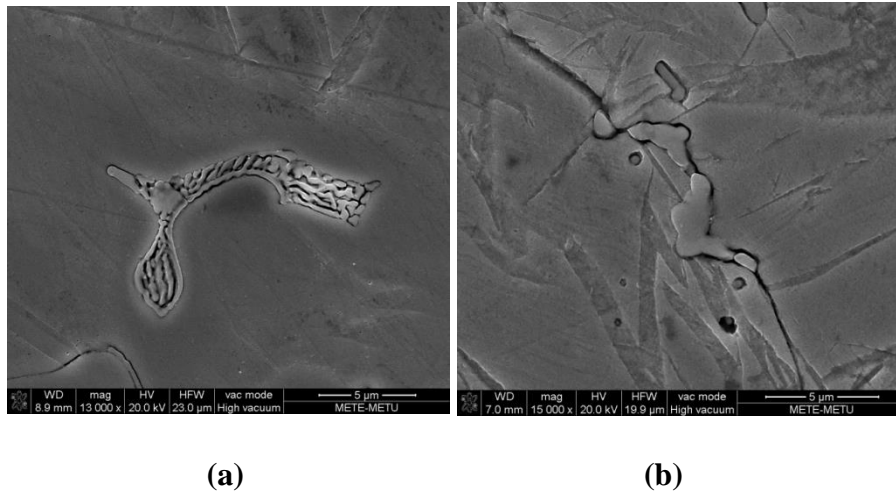


*Figure 4.29  $M_7C_3$  primary carbide structure of (a) as-cast and (b) as-rolled tool steel slabs produced by permanent copper mould casting.*

At as-cast sample and as-rolled sample, the quantity of retained austenite is approximately 59.82% and 40.68% percent respectively. It can be understood that during water atomization, the rapid solidification of AISI DC53 tool steel outcomes in full suppression of martensite phase. The retained austenite in the rapidly solidified high chromium cold work tool steel particles was very stable that did not convert to martensite even quenching in liquid nitrogen [46]. Bhargava et al. [47] recorded similar microstructure for rapidly solidified D2 tool steel using the melt spun technique. It was discovered that the austenite lattice parameter in melt-spun steel D2 steel was greater than that for  $\gamma$ -Fe due to substantial dissolution of carbon and chromium in the austenite. By comparison, AISI DC53 steel's fast solidification through thin section copper mould casting outcomes in about 40% matrix by martensite phase.

#### **4.8. Austenitization of AISI DC53**

Commercial steel optical micrographs austenitized for 1 hour at 1000°C , 1025°C , 1050°C, 1075°C , 1100°C, 1125°C, 1150°C, 1175°C (Figures 41, 42, 43, 44, 45, 46, 47, 48) demonstrates that microstructure consists of big and coarse primary carbides and martensite matrix. Hot rolling creates a banding structure of these carbides.

Moreover these coarse main carbides are very stable and dissolve entirely in matrix, at high austenitizing temperatures. The developed tool steel is entirely free of large and coarse carbides. White areas seen at the optical micrograph of steel (Figures 49, 50, 51, 52, 53, 54, 55, 56) austenitized at 1000°C , 1025°C , 1050°C, 1075°C, 1100°C, 1125°C, 1150°C, 1175°C for 1 hour are retained austenite and dark areas are martensite. The quantity of retained austenite at tool steel commercial and produced steel increases with increasing austenitizing temperature as shown in Figure 57, 58 and 59. The main reason of that is the higher the austenitizing temperature, the more carbide dissolves in the structure. Alloy elements from these carbides reduce the martensite finish temperature to lower temperatures. Therefore, with increasing austenitizing temperature, more carbide is dissolved and the retained austenite amount increases.

However, the hardness increases to a certain temperature and then decreases as shown in Figure 60. The reason for this is that first carbides dissolve and provide carbon to the structure. This increases the hardness by a certain amount. With the increasing austenitizing temperature, the matrix is saturated with carbon and the retained austenite amount begins to increase and the hardness begins to decrease. For this reason, the optimum austenitization temperature was determined as 1025°C in this study.

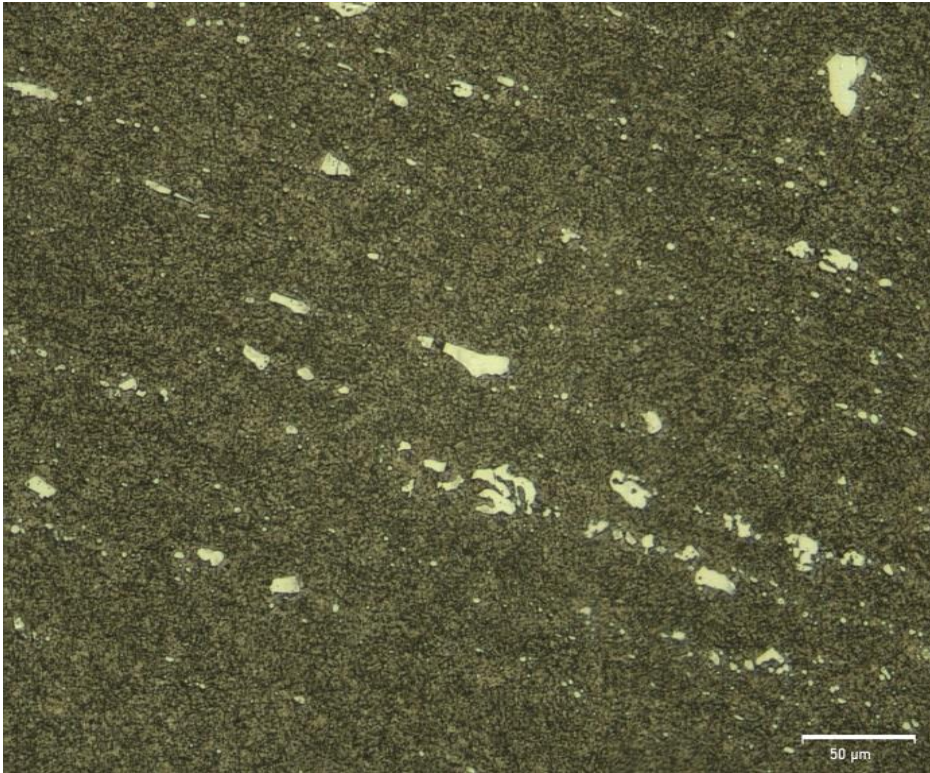


*Figure 4.30 Microstructure of commercial steel austenitized at 1000°C*

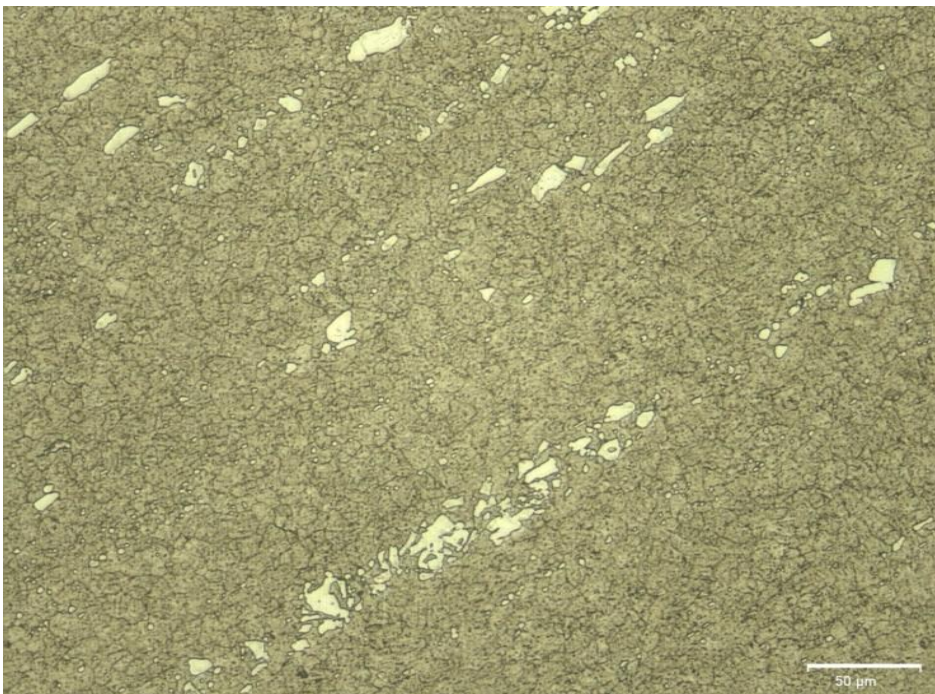


*Figure 4.31 Microstructure of commercial steel austenitized at 1025°C*



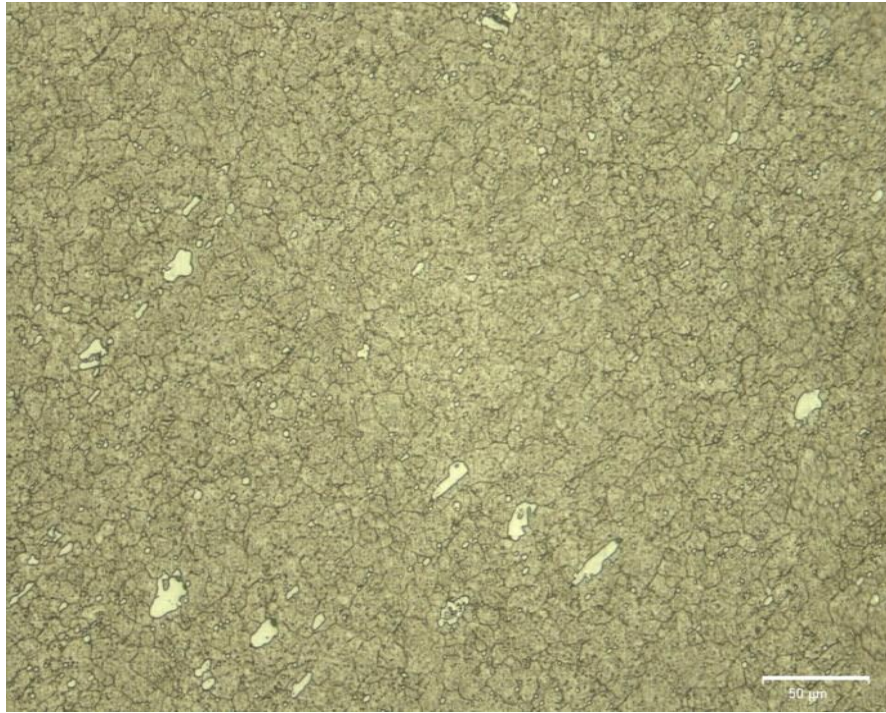


*Figure 4.32 Microstructure of commercial steel austenitized at 1050°C*

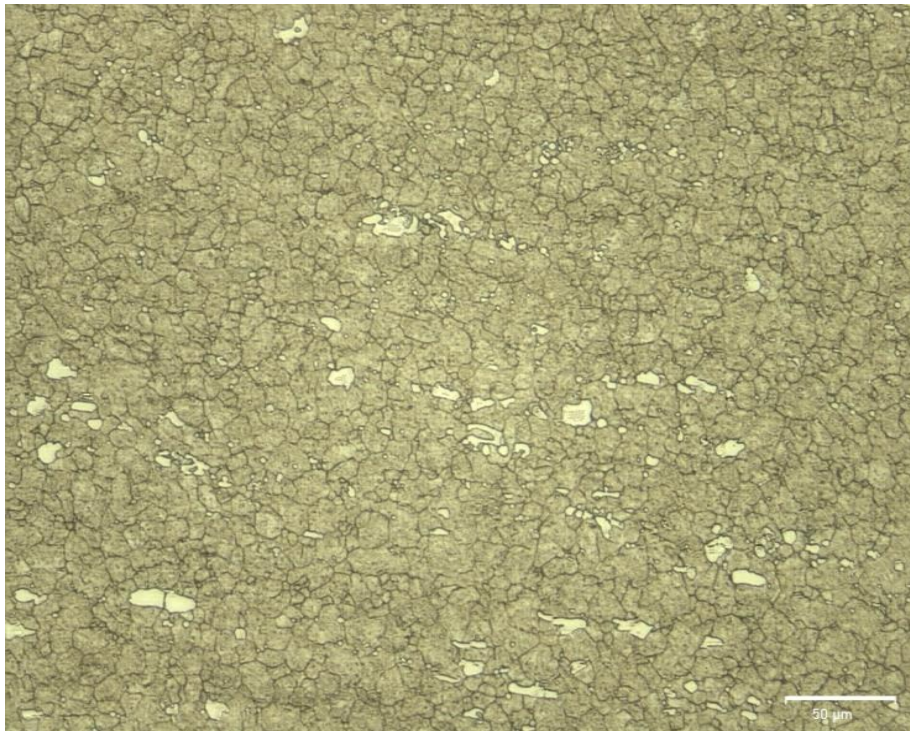


*Figure 4.33 Microstructure of commercial steel austenitized at 1075°C*

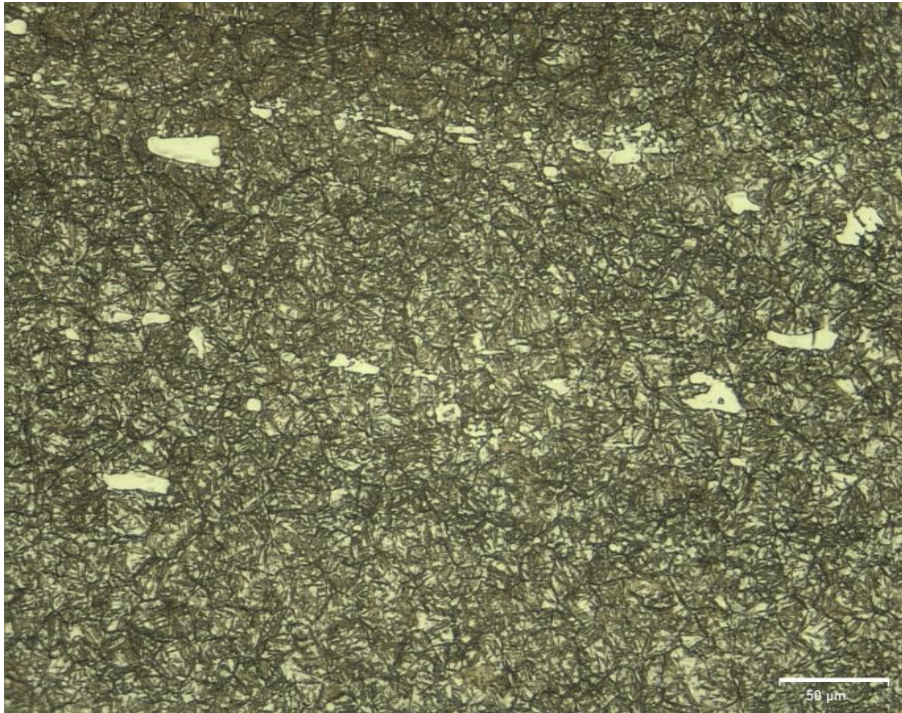


*Figure 4.34 Microstructure of commercial steel austenitized at 1100°C*

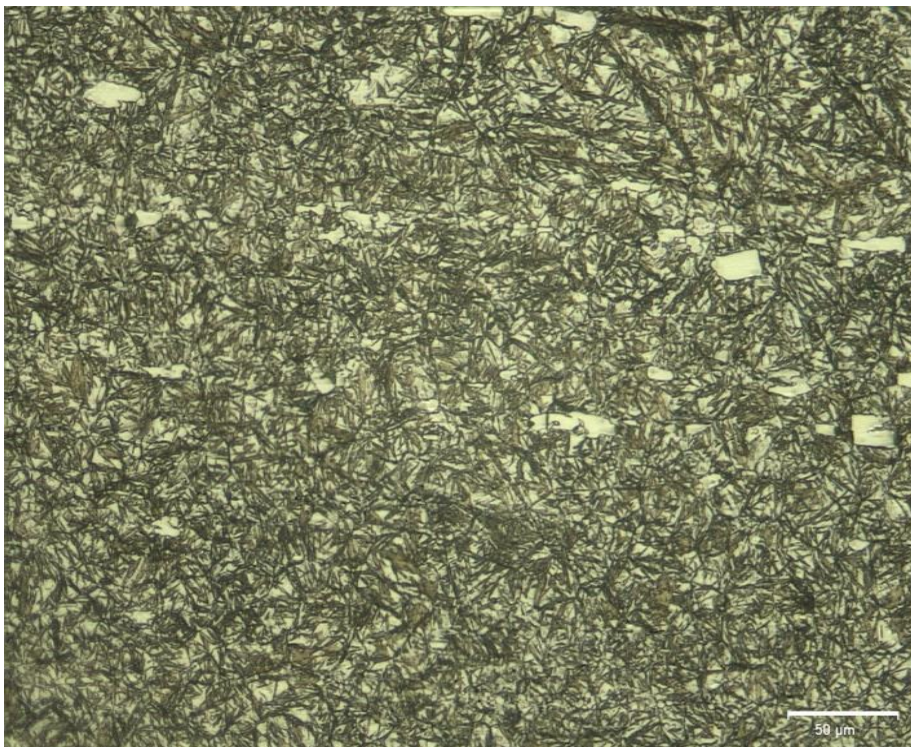


*Figure 4.35 Microstructure of commercial steel austenitized at 1125°C*

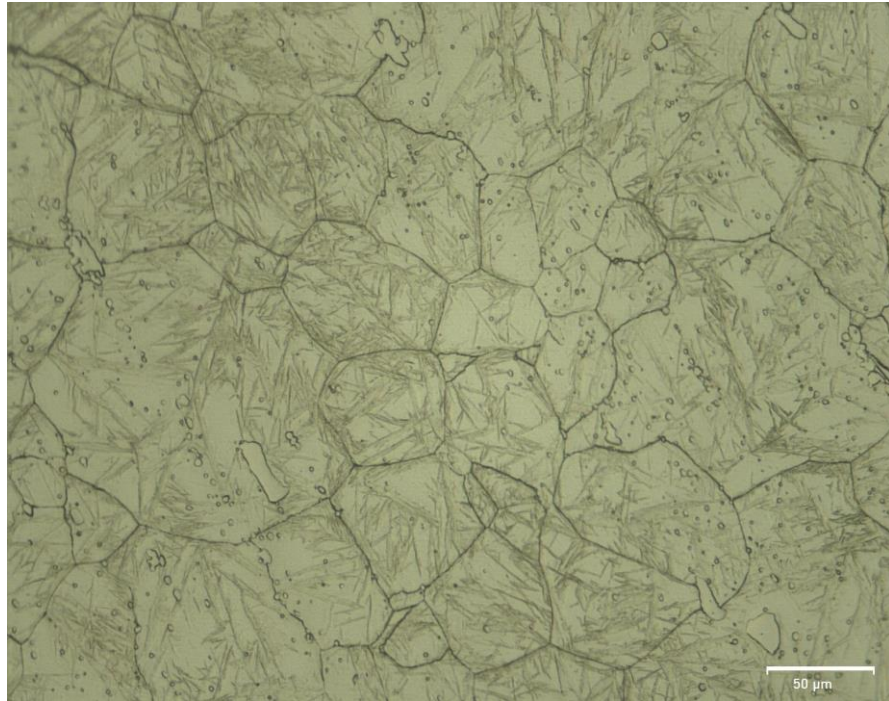


*Figure 4.36 Microstructure of commercial steel austenitized at 1150°C*

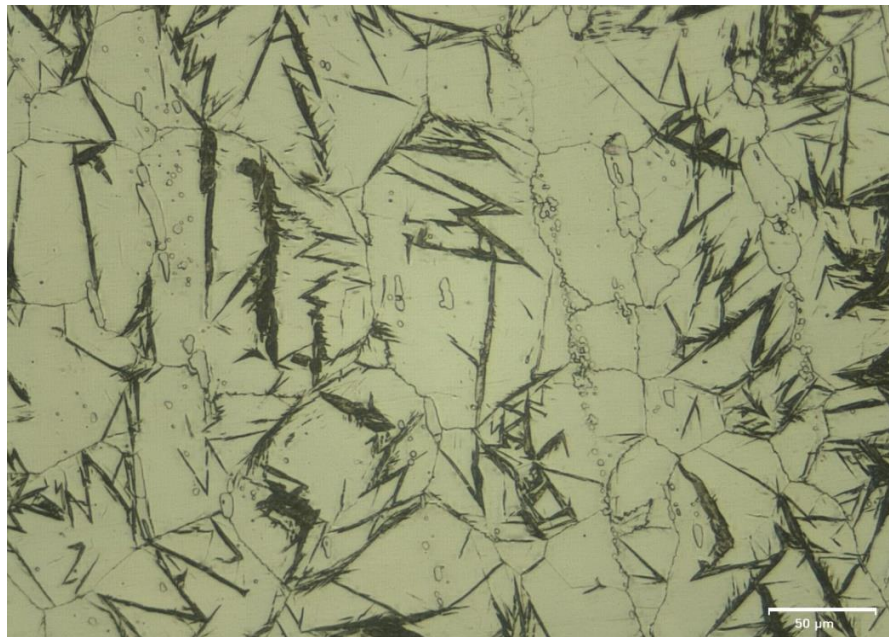


*Figure 4.37 Microstructure of commercial steel austenitized at 1175°C*

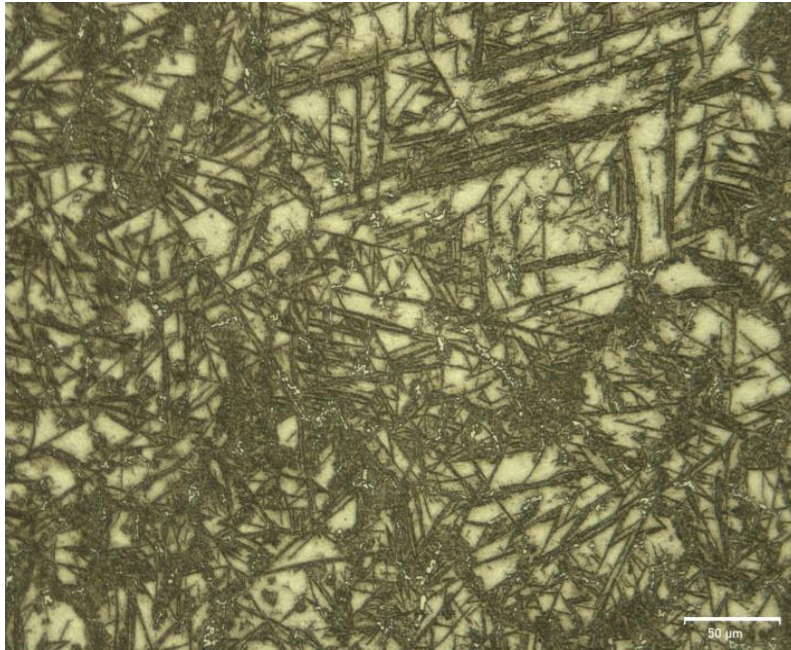


*Figure 4.38 Microstructure of developed steel austenitized at 1000°C*

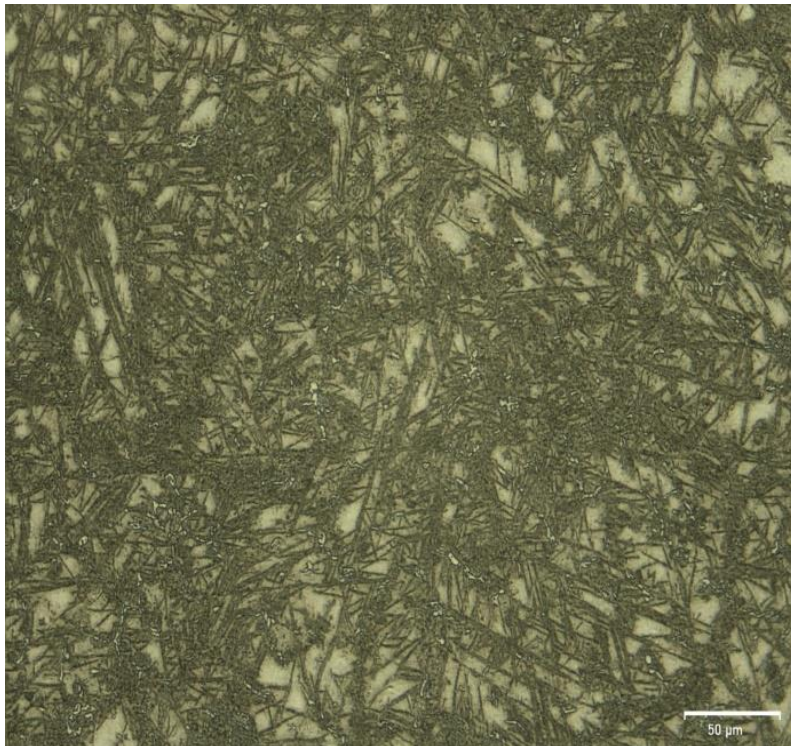


*Figure 4.39 Microstructure of developed steel austenitized at 1025°C*

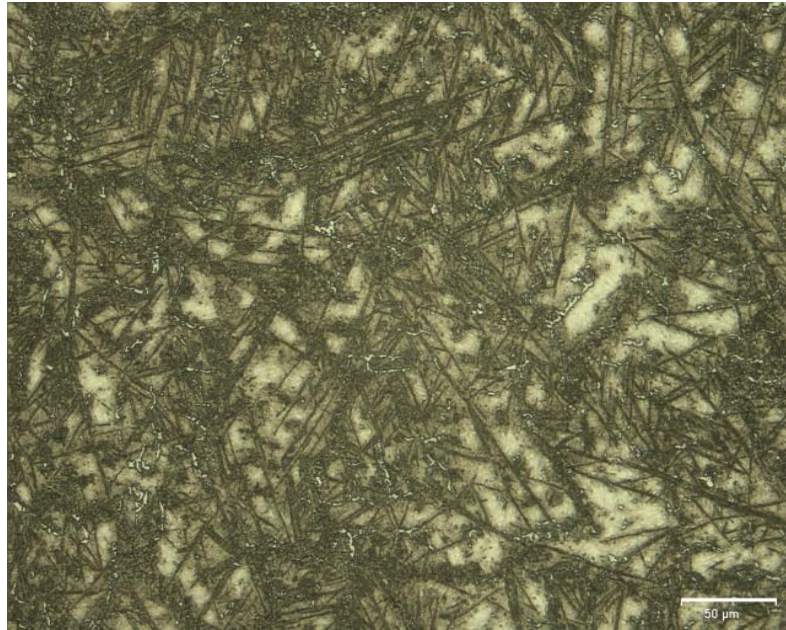


*Figure 4.40 Microstructure of developed steel austenitized at 1050°C*

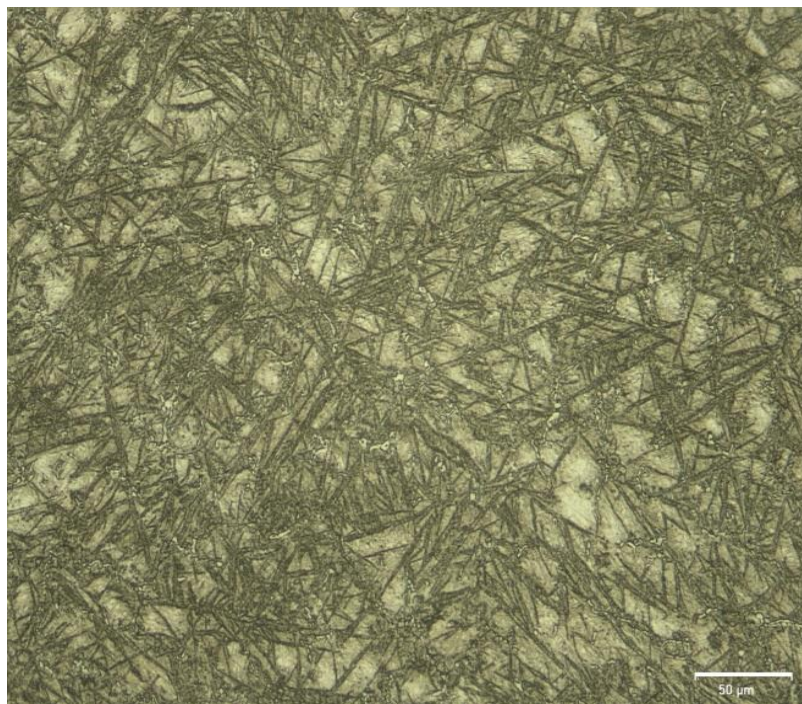


*Figure 4.41 Microstructure of developed steel austenitized at 1075°C*

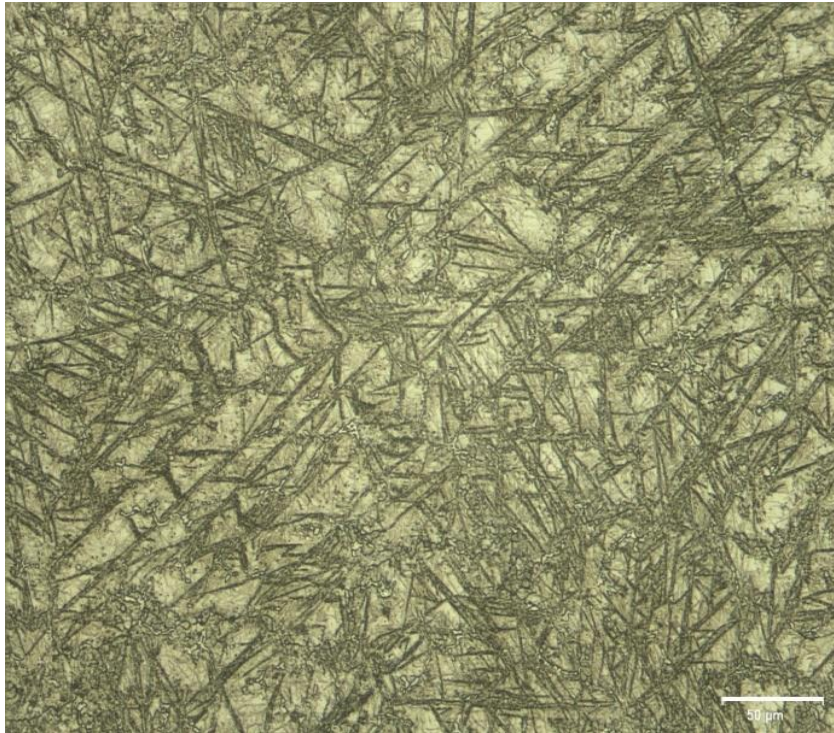


*Figure 4.42 Microstructure of developed steel austenitized at 1100°C*

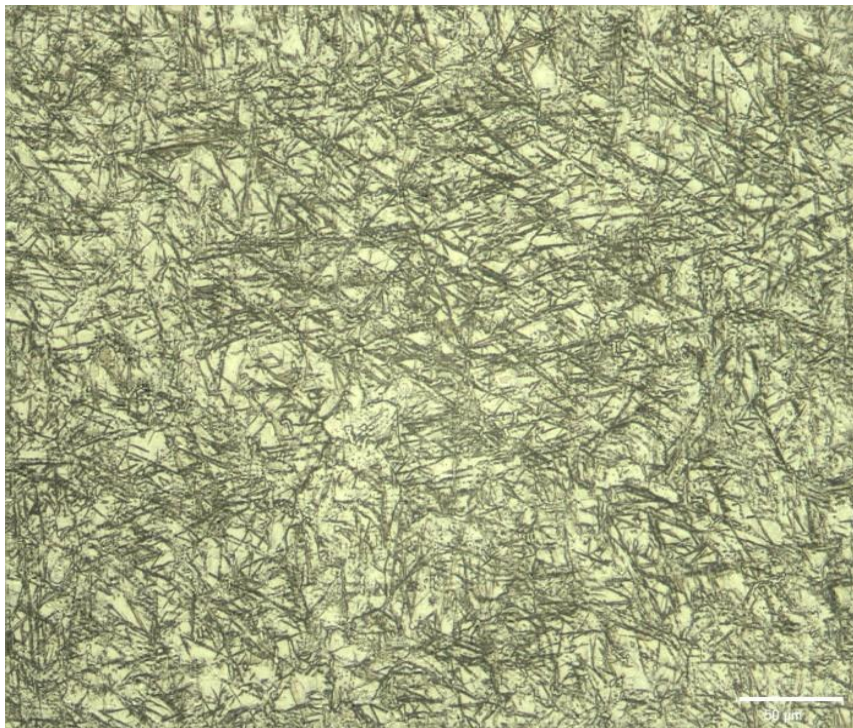


*Figure 4.43 Microstructure of developed steel austenitized at 1125°C*

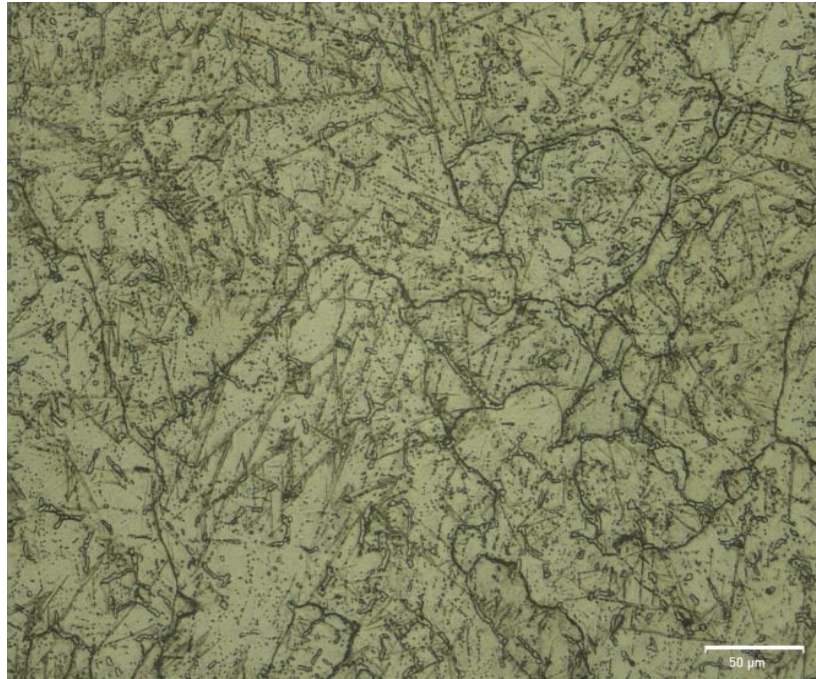


*Figure 4.44 Microstructure of developed steel austenitized at 1150°C*

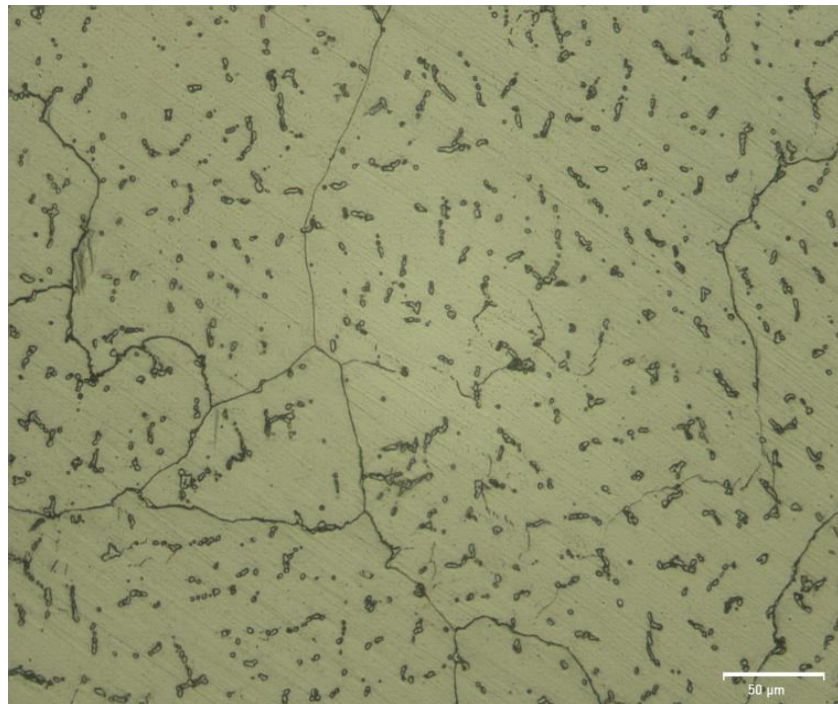


*Figure 4.45 Microstructure of developed steel austenitized at 1175°C*

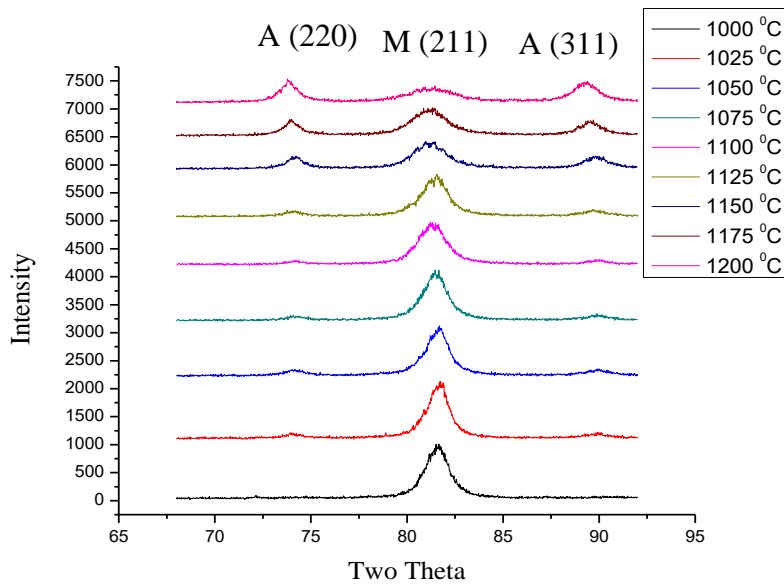


Figure 4.46 XRD patterns of commercial steel at different temperatures for 1 hour

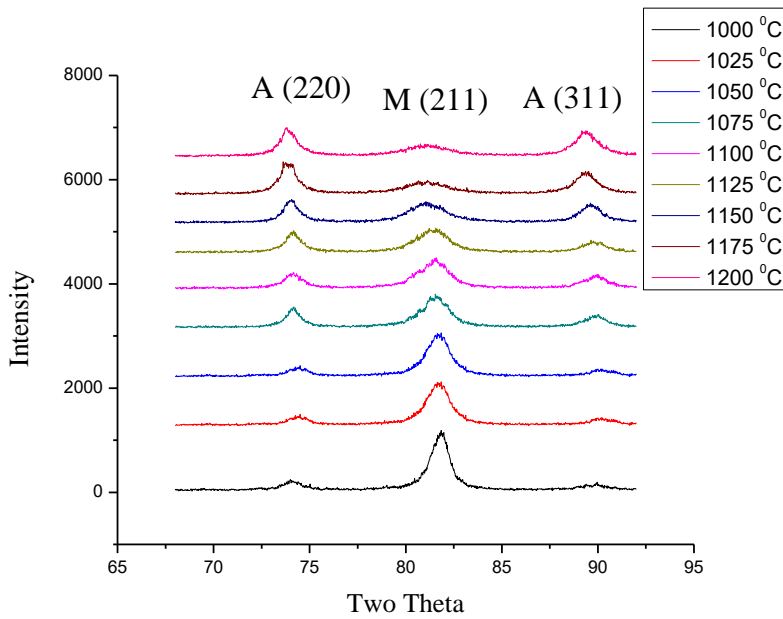


Figure 4.47 XRD patterns of austenitized new steel at different temperatures for 1 hour



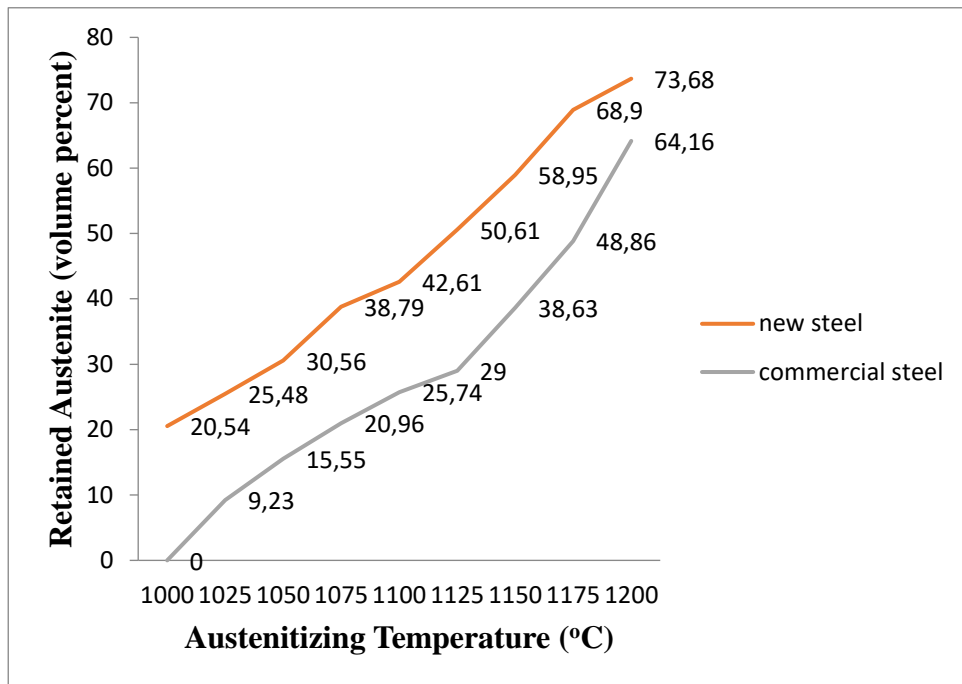


Figure 4.48 Retained austenite amount of new steel and commercial one after austenitizing heat treatments

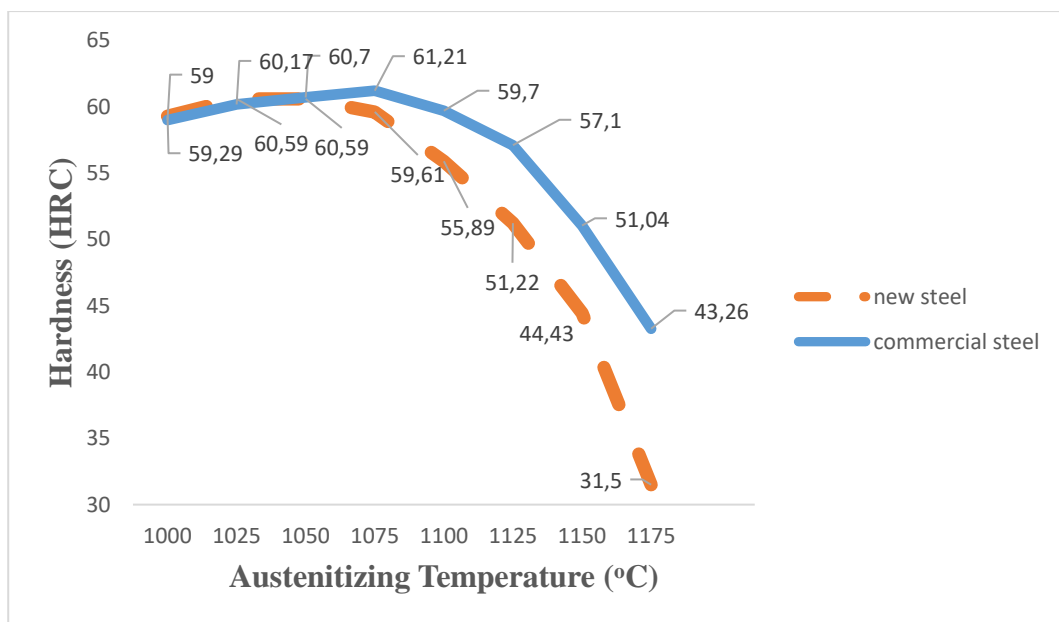
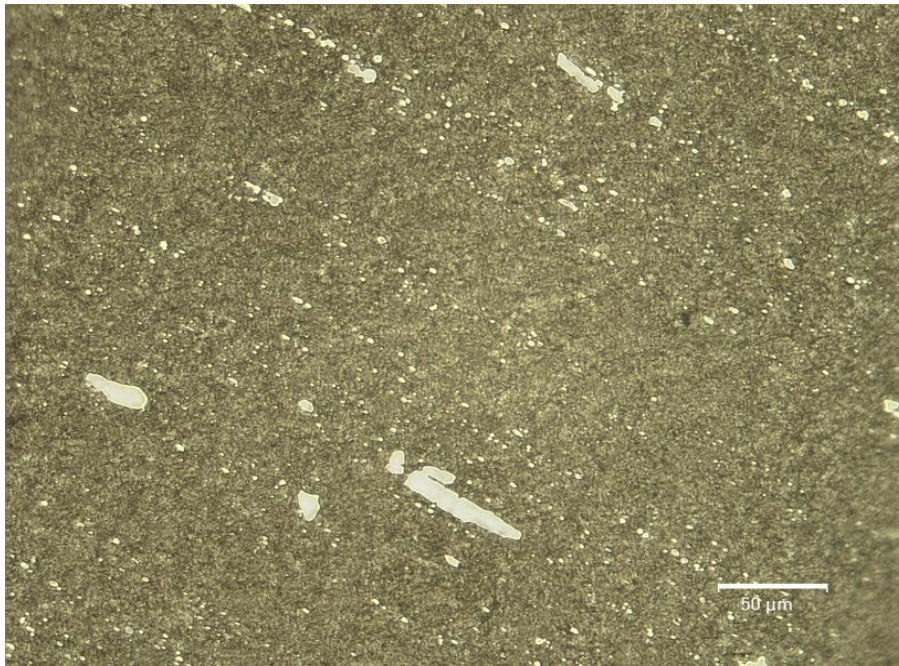


Figure 4.49 Hardness values of new steel and commercial one after austenitizing heat treatments.

#### 4.9. Microstructure & Retained Austenite Content of Tempered Steel

Optical micrographs of commercial steel austenitized for 1 hour at 1025°C and tempered twice at 525°C for 30, 60, 90 and 120 minutes (Figure 61, 62, 63, 64) demonstrates that microstructure consists of big and coarse primary carbide banding, new forming of fine carbides and tempered martensitic and bainitic matrix. Fine and more homogeneous microstructure of tempered martensite and bainite can be noted from optical tool steel micrographs austenitized at 1025°C for one hour and tempered twice at 525°C for 30, 60, 90 and 120 minutes (Figure 65, 66, 67, 68). The volumes of retained austenite commercial steel austenitized at 1025°C for 1 hour and tempered twice at 525°C for 30, 60, 90 and 120 minutes are about 2.72%, 1.17%, 0% and 0% respectively. The volumes of retained austenite of tool steel produced austenitized at 1025°C for 1 hour and tempered twice at 525°C for 30, 60, 90 and 120 minutes are approximately 8.96%, 2.43%, 1.55% and 0% respectively.



*Figure 4.50 Microstructure of commercial steel austenitized at 1025°C for 1 hour and tempered twice at 525°C for 30 minutes*

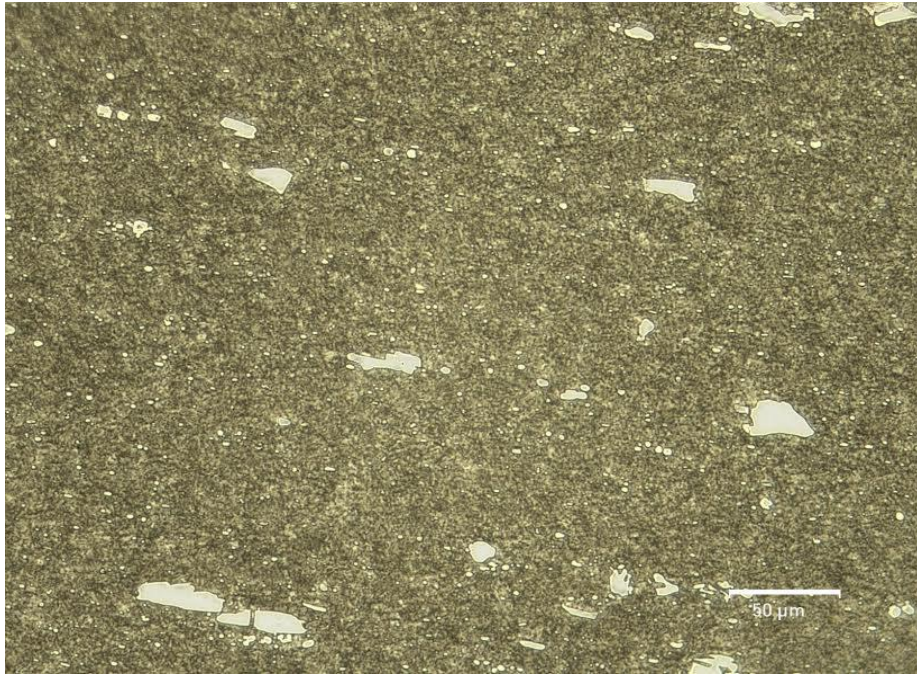


*Figure 4.51 Microstructure of commercial steel austenitized at 1025°C for 1 hour and tempered twice at 525°C for 60 minutes*

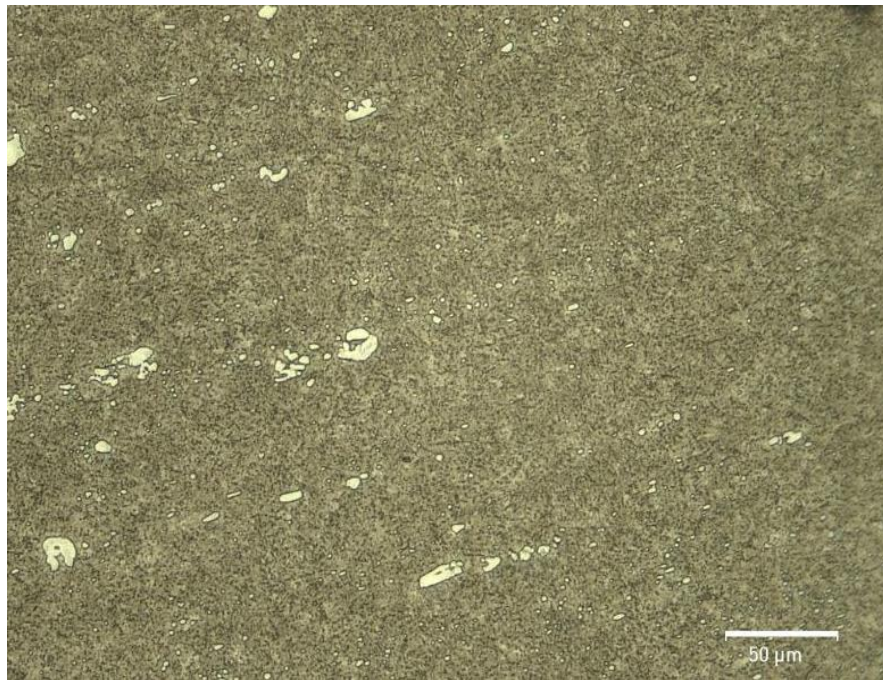


*Figure 4.52 Microstructure of commercial steel austenitized at 1025°C for 1 hour and tempered twice at 525°C for 90 minutes*

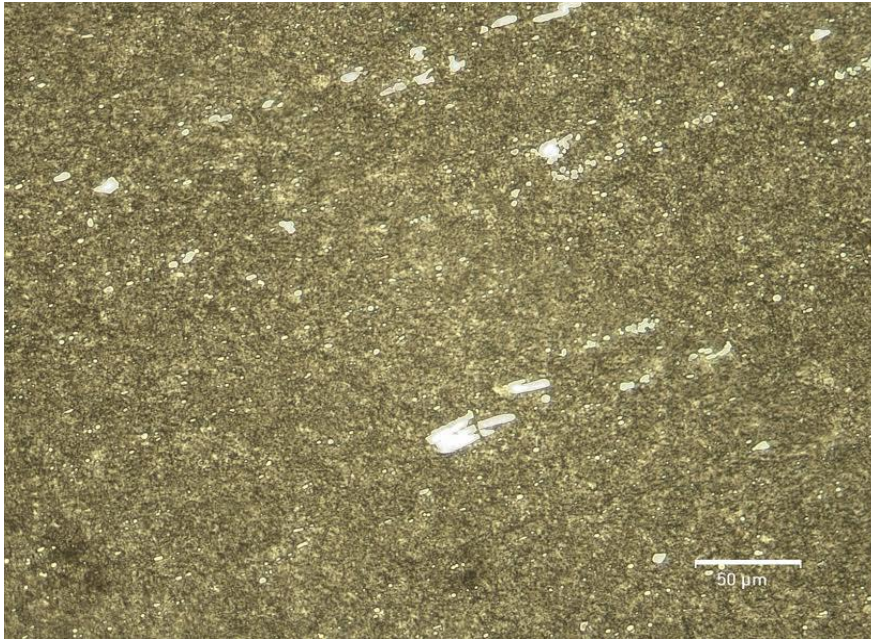


*Figure 4.53 Microstructure of commercial steel austenitized at 1025°C for 1 hour and tempered twice at 525°C for 120 minutes*

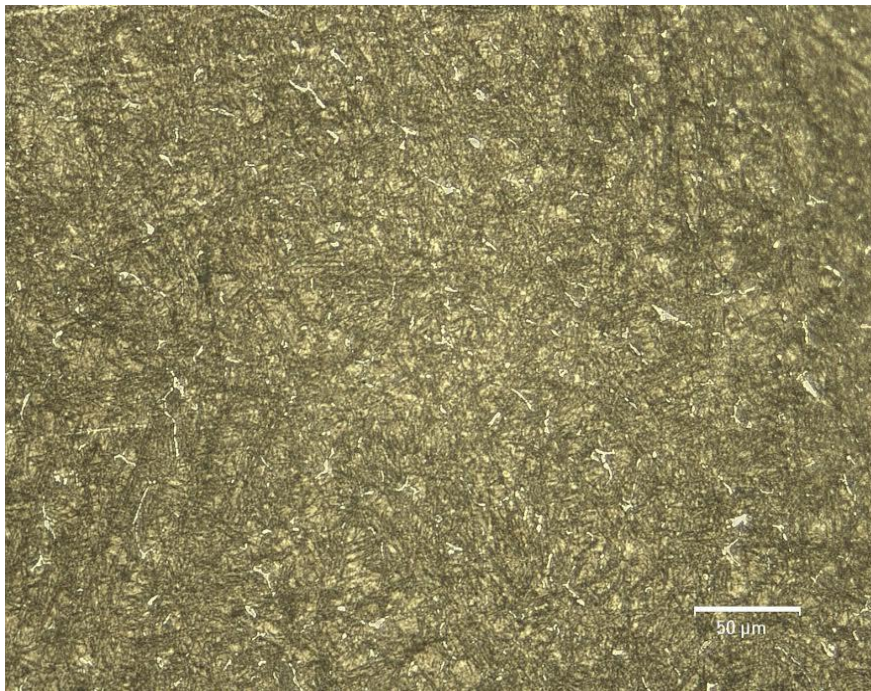


*Figure 4.54 Microstructure of developed steel austenitized at 1025°C for 1 hour and tempered twice at 525°C for 30 minutes*

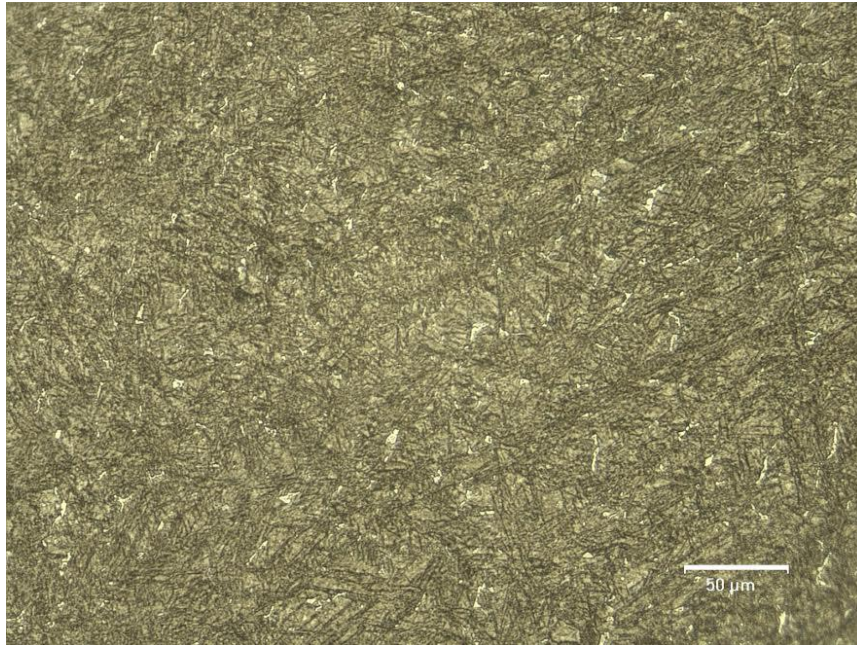


*Figure 4.55 Microstructure of developed steel austenitized at 1025°C for 1 hour and tempered twice at 525°C for 60 minutes*

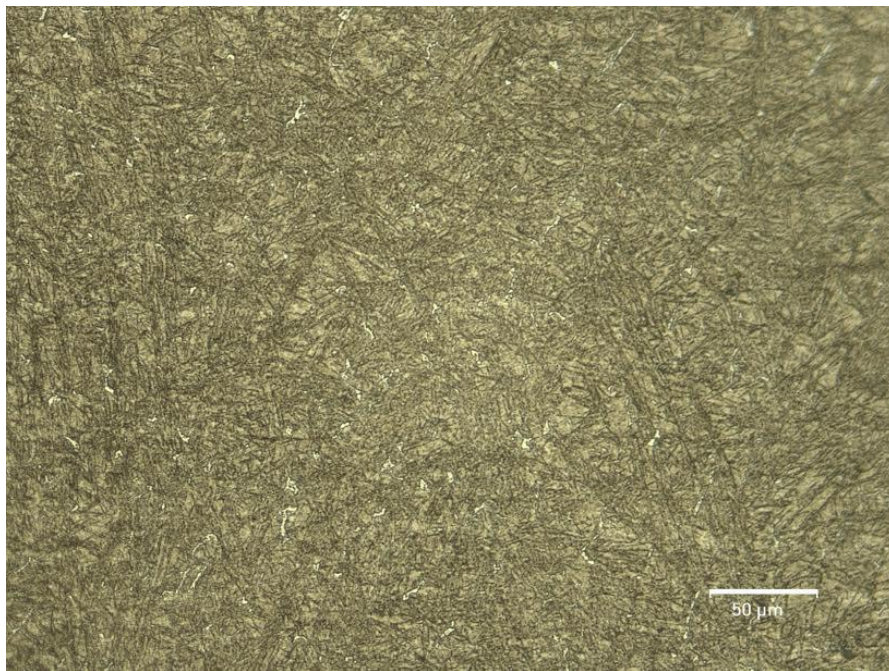


*Figure 4.56 Microstructure of developed steel austenitized at 1025°C for 1 hour and tempered twice at 525°C for 90 minutes*

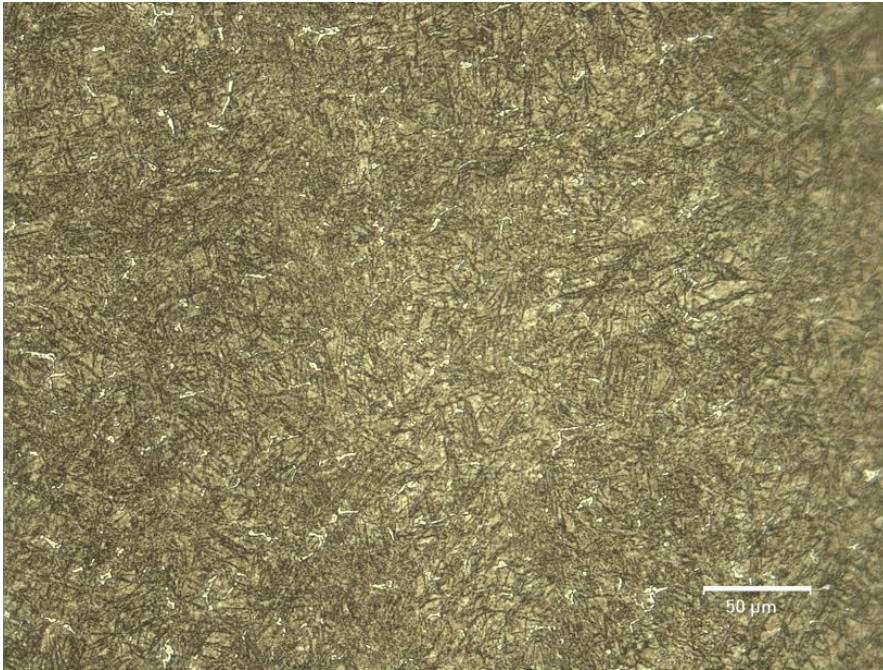


*Figure 4.57 Microstructure of developed steel austenitized at 1025°C for 1 hour and tempered twice at 525°C for 120 minutes*

#### **4.10. Hardness**

Hardness reduces for two steels (the tool steel developed and commercial one) (Figure 69) up to 60 minutes two tempering. Due to secondary hardening phenomena, hardness of tool steel developed rises after 60 minutes. After 90 minutes of two tempering, secondary hardening was noted for commercial steel. Due to high volume proportion of dissolving carbon atoms in matrix rather than forming carbides, secondary hardening of tool steel developed is seen sooner than commercial steel. Hardness values of the AISI DC53 steels produced by traditional method are in the range of 53-55 HRC after austenitization for 1 hour 1025°C and quenched in compressed air and tempered twice for 120 minutes at 525°C. Permanent mould cast AISI DC53 after homogenization at 1150°C and immediately hot rolling and austenitized at 1025°C for one hour then quenched by compressed air and tempered twice at 525°C for 120 mins have hardness values in the range of 55-57 HRC. In addition, new steel hardness values for all tempering times are greater than commercial steel hardness values.

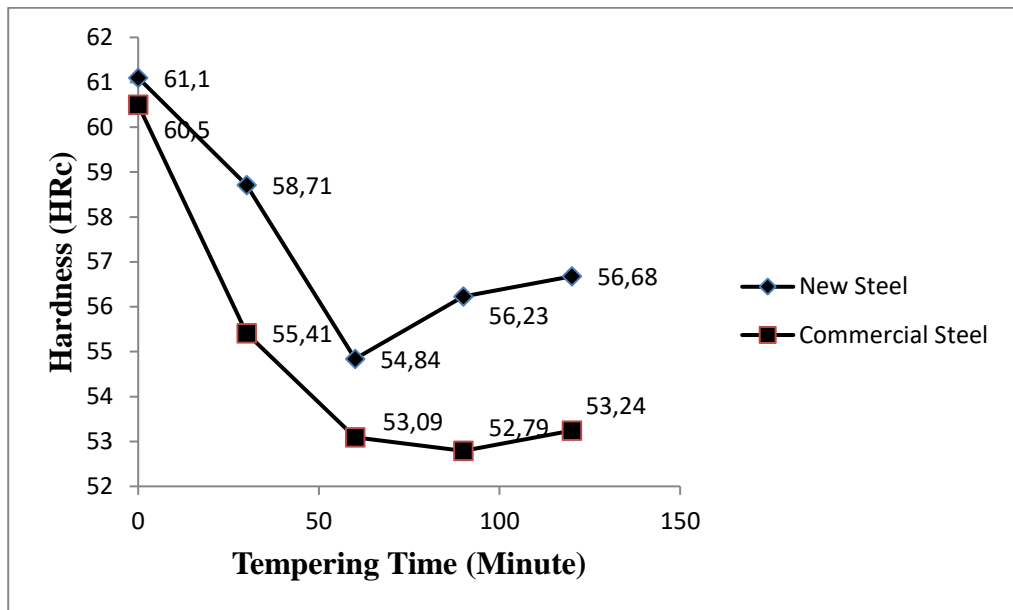


Figure 4.58 The hardness values of the tool steel (new steel) developed and commercial one after tempering heat treatments.





## CHAPTER 5

### CONCLUSION

Studies have shown that tool steel product with moderate and high cooling rates have a more homogeneous and segregation-free microstructure than commercial AISI DC53 tool steel. It can be concluded after experiments:

(1) The secondary dendrite arm spacing of sand and copper wedge steel samples showed a roughly linear relationship with the section thickness

(2) The sand and copper wedge samples' cooling rates showed an approximately second-order exponential relationship with the section thickness.

(3) The solidification rates of the sand and copper wedge samples obtained by Novacast casting simulation program differ from the values calculated by using the empirical formula in the literature.

(4) High solidification rates trigger a big quantity of metastable (or residual) austenite present in the steel at room temperature, and the quantity of retained austenite increases as the solidification rate increases.

(5) High rates of solidification trigger nucleation of the primary carbides. In addition, the existing solid phases do not have enough time to grow and they have been spread homogeneously and fine. The size of the primary carbide declines as the solidification rate increases.

(6) Although in rapidly solidified AISI DC53 steel, dendritic, refined equiaxed and compound (a mixture of dendritic and refined equiaxed) microstructures were observed, only equiaxed grains were detected in fast solidified AISI DC53 steel.

(7) With moderate and high cooling levels, the tool steel powders and slabs had more homogeneous and fine primary carbides than the commercially made AISI DC53 steel.

(8) AISI DC53 tool steel was rapidly solidified by water atomization, full martensite phase suppression happened. X-ray diffraction was detected about 59.82 percent retained austenite (metastable) phase at room temperature after rapid solidification of AISI DC53 tool steel by thin section casting

(9) No primary coarse  $M_7C_3$  carbides were observed in the powder microstructure produced by water atomization, but an interdendritic carbide network with a thickness of 2–4  $\mu\text{m}$  was revealed. In addition, carbides were found at austenite and martensite grain boundaries in the microstructure of slabs generated by permanent copper mould casting. These lamellar carbides having the range of 5 – 15  $\mu\text{m}$  were determined to be coarser than carbides observed in tool steel powder matrix

(10) Solidification by permanent copper mould casting caused more carbon atoms to be dissolved in the matrix instead of forming carbides and, in this work, after tempering commercial and developed tool steel, the hardness values of the tool steel developed by permanent copper casting are higher than that of commercial steel for all tempering times.

## CHAPTER 6

### SUGGESTIONS FOR FUTURE WORK

Following items should be performed in the scope of future works:

- i)** Experiments should be performed using real thermocouples together with the thermocouples used in the simulation.
  
- ii)** Experiments related to the toughness of new fast solidified steel should be conducted.
  
- iii)** By using cooling curve, the latent heat and fraction of carbides of AISI DC53 cold work tool steel can be calculated.



## REFERENCES

- [1] Berger, C., Scheerer, H., & Ellermeier, J. (2010). Modern materials for forming and cutting tools - Overview. *Materials Science and Materials Engineering*, 41(1), 5–17. <http://doi.org/10.1002/mawe.200900529>
- [2] G.A. Roberts, G. Krauss, R. Kennedy, Tool Steels, 5th edition, American Society for Metals, Metals Park, Ohio, 1998.
- [3] Fukaura, K., Yokoyama, Y., Yokoi, D., Tsujii, N., & Ono, K. (2004). Fatigue of cold work tool steels: Effect of heat treatment and carbide morphology on fatigue crack formation, life, and fracture surface observations. *Metallurgical and Materials Transactions a-Physical Metallurgy and Materials Science*, 35A (4), 1289–1300. <https://doi.org/10.1007/s11661-004-0303-5>
- [4] Blaha, J., Kremaszky C., Werner E.A. Carbide distribution effects in cold work tool steels. Proc. of 6th International Tooling Conference, Karlstad University, Sweden (September 2002), pp. 289-298
- [5] P. Grgac, R. Moravcik, M. Kusy, I. Toth, M. Miglierini, and E. Illekova, “Thermal stability of metastable austenite in rapidly solidified chromium-molybdenum-vanadium tool steel powder,” *Mater. Sci. Eng. A*, vol. 375–377, no. 1–2 SPEC. ISS. pp. 581–584 (2004). <https://doi.org/10.1016/j.msea.2003.10.036>
- [6] P. Delshad Khatibi, A. Ilbagi, and H. Henein, “Microstructural Investigation of D2 Tool Steel during Rapid Solidification using Impulse Atomization,” in *The Minerals, Metals & Materials Society (TMS)* (2011), pp. 531–538. <http://dx.doi.org/10.1002/9781118062111.ch60>
- [7] J. G. Zhang, H. S. Shi, and D. S. Sun, “Research in spray forming technology and its applications in metallurgy,” in *Journal of Materials Processing Technology*, vol. 138, no. 1–3, pp. 357–360 (2003). [https://doi.org/10.1016/S0924-0136\(03\)00098-0](https://doi.org/10.1016/S0924-0136(03)00098-0)

- [8] J. G. Zhang, H. Bin Xu, H. S. Shi, J. S. Wu, and D. S. Sun, "Microstructure and properties of spray formed Cr12MoV steel for rolls," *J. Mater. Process. Technol.*, vol. 111, no. 1–3, pp. 79–84 (2001). [https://doi.org/10.1016/S0924-0136\(01\)00516-7](https://doi.org/10.1016/S0924-0136(01)00516-7)
- [9] Y. Lin, K. M. McHugh, Y. Zhou, and E. J. Lavernia, "Microstructure and hardness of spray-formed chromium-containing steel tooling," *Scr. Mater.*, vol. 55, no. 7, pp. 581–584 (2006). <https://doi.org/10.1016/j.scriptamat.2006.06.020>
- [10] J. Hamill, C. Schade, and N. Myers, "Water Atomized Fine Powder Technology," *Proc. 2000 Powder Metall. World Congr. JPMA*, pp. 367–370 (2000).
- [11] Li, S., Xie, Y., & Wu, X. (2010). Hardness and toughness investigations of deep cryogenic treated cold work die steel. *Cryogenics*, 50(2), 89–92. <https://doi.org/10.1016/j.cryogenics.2009.12.005>
- [12] Advanced High Strength Steel (AHSS). Application Guidelines. Version 4.1. International Iron & Steel Institute. Committee on Automotive Applications, June 2009. [www.worldautosteel.org](http://www.worldautosteel.org).
- [13] Picas, I.; Hernandez, R.; Casellas, D.; Valls, I.; Strategies to increase the tool performance in punching operations of UHSS. R. Kollek (Ed.), Proc IDDRG, Graz, Austria (2010), pp. 325-334.
- [14] L. Johnson: Contact Mechanics, Cambridge University Press, Cambridge, United Kingdom, 1985.
- [15] Gonzalez, E.M. Detection of Failure Mechanisms of Tool Steels by means of Acoustic Emission Technique, Doctoral Thesis, 2013
- [16] Davis, J. R., *Tool Materials*, ASM, 1995
- [17] Geller, Y. *Tool Steels*, Mir Publishers Moscow, 1978
- [18] Vogel, C. et al. *Metallurgi for Ingeniører* 6th edit. 1993

- [19] Wilson, R. *Metallurgy and Heat Treatment of Tool Steels*, McGraw-Hill Book Company (UK) Limited, 1975
- [20] H. Kim, J. Y. Kang, D. Son, T. H. Lee, and K. M. Cho, “Evolution of carbides in cold-work tool steels,” *Mater. Charact.*, 2015.
- [21] Porter, D. et al. *Phase Transformations in Metals and Alloys 2nd edit.* Chapman & Hall, 1992
- [22] Zackery, V. *Decomposition of Austenite by Diffusional Processes*, John Wiley and Sons, 1962
- [23] Møller, P. *Avanceret Teknologi*, Teknisk Forlag, 1998.
- [24] Hull, D. et al. *Introduction to Dislocations 3rd edit*, Butterworth/Heinemann1984]
- [25] Højerslev, C. (2001). Tool steels. Roskilde: Risø National Laboratory. Denmark. Forskningscenter Risoe. Risoe- R, No. 1244(EN)
- [26] <http://www.steeldata.info/carbides/demo/data/1232.html>
- [27] H.K.D.H. Bhadeshia, *Bainite in Steels*, London: IOM commercial ltd, 2001.
- [28] G.R. Speich, W.C. Leslie, “Tempering of Steel,” *Metallurgical Transactions*, vol. 3, no. May, pp. 1043-1054, 1972.
- [29] J. Akre, F. Danoix, H. Leitner, P. Auger, “The morphology of secondaryhardening carbides in a martensitic steel at the peak hardness by 3DFIM,” *Ultramicroscopy*, no. 109, pp. 518-523, 2009.
- [30] K. Stiller, L.E. Svensson, P.R. Howell, W. Rong, H.O. Andren, G.L. Dunlop, “High Resolution Microanalytical study of precipitation in a Powder Metallurgical High-Speed Steel,” *Acta Metall*, vol. 32, pp. 1457- 1467, 1984.

- [31] Rehan, M. A. Microstructure and mechanical properties of a 5 wt. % Cr cold work tool steel - Influence of heat treatment procedure. Licentiate Thesis Production Technology 2017 No. 18
- [32] [https://www.uddeholm.com/app/uploads/sites/40/2017/11/sleipner\\_eng\\_p\\_R1609\\_e11.pdf](https://www.uddeholm.com/app/uploads/sites/40/2017/11/sleipner_eng_p_R1609_e11.pdf)
- [33] Cullity, B. D., & Stock, S. R. (2001). *Elements of X-ray diffraction, 3rd edition*. Prentice Hall. <https://doi.org/citeulike-article-id:3998040>
- [34] GUO, W., & ZHU, M. yong. (2009). Characteristic Parameters for Dendritic Microstructure of Solidification during Slab Continuous Casting. *Journal of Iron and Steel Research International*, 16(1), 17–21. [https://doi.org/10.1016/S1006-706X\(09\)60004-2](https://doi.org/10.1016/S1006-706X(09)60004-2)
- [35] Zhang, J. G., Xu, H. Bin, Shi, H. S., Wu, J. S., & Sun, D. S. (2001). Microstructure and properties of spray formed Cr12MoV steel for rolls. *Journal of Materials Processing Technology*, 111(1–3), 79–84. [https://doi.org/10.1016/S0924-0136\(01\)00516-7](https://doi.org/10.1016/S0924-0136(01)00516-7)
- [36] Lin, Y., McHugh, K. M., Zhou, Y., & Lavernia, E. J. (2006). Microstructure and hardness of spray-formed chromium-containing steel tooling. *Scripta Materialia*, 55(7), 581–584. <https://doi.org/10.1016/j.scriptamat.2006.06.020>
- [37] Li, S., Xie, Y., & Wu, X. (2010). Hardness and toughness investigations of deep cryogenic treated cold work die steel. *Cryogenics*, 50(2), 89–92. <https://doi.org/10.1016/j.cryogenics.2009.12.005>
- [38] A. Bose, *Advances in Particulate Materials*, 1995 Butterworth-Heinemann, Boston.
- [39] P. Grgac, M. Liptak, M. Behulova, L. Caplovic, H. G. Lindenkreuz, and W. Löser, “Influence of melt undercooling on the microstructure of levitated Cr-Mo-V



tool steel,” *Mater. Sci. Eng. A*, vol. 448–451, pp. 658–661 (2007).  
<https://doi.org/10.1016/j.msea.2006.02.428>

[40] T. Y. Hsu (Xu Zuyao) , *Martensitic Transformation and Martensite*, Science Press, Beijing, 1999 (second version).

[41] G. N. Haidemenopoulos, M. Grujicic, G. B. Olson, and M. Cohen, “Thermodynamics-based alloy design criteria for austenite stabilization and transformation toughening in the FeNiCo system,” *J. Alloys Compd.*, vol. 220, no. 1–2, pp. 142–147, 1995.

[42] Q. Meng, Y. Rong, and T. Y. Hsu, “Nucleation barrier for phase transformations in nanosized crystals,” *Phys. Rev. B - Condens. Matter Mater. Phys.*, vol. 65, no. 17, pp. 1–7, 2002.

[43] J. X. Zou, T. Grosdidier, K. M. Zhang, B. Gao, S. Z. Hao, and C. Dong, “Microstructures and phase formations in the surface layer of an AISI D2 steel treated with pulsed electron beam,” *J. Alloys Compd.*, vol. 434–435, no. SPEC. ISS., pp. 707–709 (2007). <https://doi.org/10.1016/j.jallcom.2006.08.280>

[44] R. Colaço and R. Vilar, “On the influence of retained austenite in the abrasive wear behaviour of a laser surface melted tool steel,” in *Wear*, vol. 258, no. 1–4 SPEC. ISS., pp. 225–231 (2005). <https://doi.org/10.1016/j.wear.2004.09.029>

[45] M. Pleterški, T. Muhič, D. Klobčar, and L. Kosec, “Microstructural evolution of a cold work tool steel after pulsed laser remelting,” *Metalurgija*, vol. 51, no. 1 (2012).

[46] P. Delshad Khatibi, A. Ilbagi, and H. Henein, “Microstructural Investigation of D2 Tool Steel during Rapid Solidification using Impulse Atomization,” in *The Minerals, Metals & Materials Society (TMS)*, 2011, pp. 531–538.

[47] A.K. Bhargava, A.N. Tiwari, Effect of rapid solidification and heat treatment on D2 steel, *International Journal of Rapid Solidification*. 7 (1992) 51–66



## CURRICULUM VITAE

### PERSONAL INFORMATION

Surname, Name : Çardaklı, İsmail Seçkin  
Nationality : Turkish (TC)  
Date and Place of Birth : 1 February 1982, Ankara  
Phone : +90 505 929 14 17  
E-mail : cardakli@atauni.edu.tr

### EDUCATION

Degree	Institution	Year of Graduation
MS	METU Met. and Mat. Engineering	2011
BS	METU Met. and Mat. Engineering	2005
High School	Etlik High School, Ankara	2000

### WORK EXPERIENCE

Year	Place	Enrollment
2018-Present	Atatürk University, Erzurum	Research Assistant
2007 September	METU, Ankara	Research Assistant

### FOREIGN LANGUAGES

Advanced English

### PUBLICATIONS

1. İsmail Seçkin Çardaklı & Ali Kalkanlı (2019) Refinement of primary carbides in AISI DC 53 cold work tool steel by thin section copper permanent mould casting and water atomization, International Journal of Cast Metals Research, 32:3, 145-153, DOI:10.1080/13640461.2019.1579483
2. İsmail Seçkin Çardaklı & Ali Kalkanlı (2019) Effect of solidification rate on microstructure and primary carbides of AISI DC 53 cold work tool steel, China Foundry 16: 211. <https://doi.org/10.1007/s41230-019-8134-6>